Chem Catalysis

CellPress

Article

Photosensitized activation of diazonium derivatives for C–B bond formation

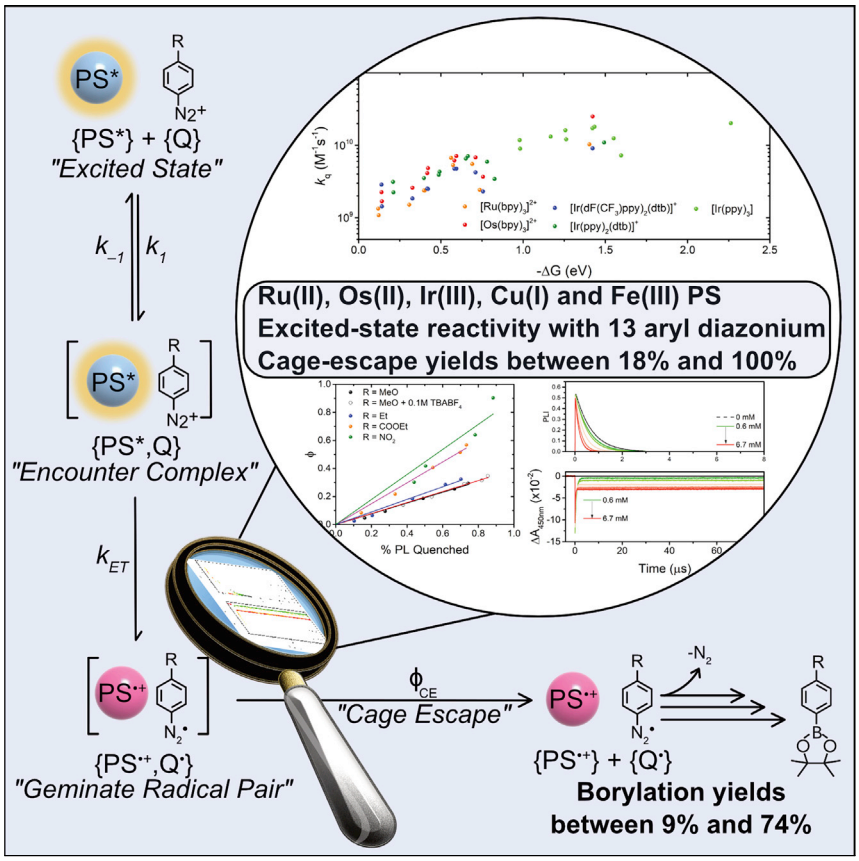

The excited-state reactivity of nine rare and earth-abundant photosensitizers with a series of aryl diazonium derivatives was investigated by means of steady-state and time-resolved spectroscopic techniques. The efficiency with which the oxidized and reduced species separate after electron transfer (i.e., the cage-escape yields) was quantified with several photosensitizers and ranged from 18% to 100%. Fe(III) photosensitizers exhibited both light and dark reactivity with aryl diazonium salts. A novel kinetic model was developed to account for these observations.

Alexia Ripak, Simon De Kreijger, Renato N. Sampaio, ..., Uttam K. Tambar, Benjamin Elias, Ludovic Troian-Gautier

ludovic.troian@uclouvain.be

Highlights

Excited-state reactivity of nine photosensitizers with 13 aryl diazonium salts

Cage-escape yields quantified and ranged from 18% to 100%

Kinetic model developed to explain dark reactivity of Fe(III) photosensitizers

Photo-induced borylation reaction with yields between 9% and 74%

Ripak et al., Chem Catalysis 3, 100490
February 16, 2023 © 2022 Elsevier Inc.
https://doi.org/10.1016/j.checat.2022.100490

Please cite this article in press as: Ripak et al., Photosensitized activation of diazonium derivatives for C–B bond formation, Chem Catalysis (2022), https://doi.org/10.1016/j.checat.2022.100490

Chem Catalysis

CellPress

Article

Photosensitized activation of diazonium derivatives for C–B bond formation

Alexia Ripak,[1] Simon De Kreijger,[1] Renato N. Sampaio,[2] Cooper A. Vincent,[3] Émilie Cauët,[4] Ivan Jabin,[5] Uttam K. Tambar,[3] Benjamin Elias,[1] and Ludovic Troian-Gautier[1,6,*]

SUMMARY

Aryl diazonium salts are ubiquitous building blocks in chemistry, as they are useful radical precursors in organic synthesis as well as for the functionalization of solid materials. They can be reduced electrochemically or through a photo-induced electron transfer reaction. Here, we provide a detailed picture of the ground- and excited-state reactivity of a series of nine rare and earth-abundant photosensitizers with 13 aryl diazonium salts, which also included three macrocyclic calix[4]arene tetradiazonium salts. Nanosecond transient absorption spectroscopy confirmed the occurrence of excited-state electron transfer and was used to quantify cage-escape yields (i.e., the efficiency with which the formed radicals separate and escape the solvent cage). Cage-escape yields were large; they increased when the driving force for photo-induced electron transfer increased and also tracked with the C–N_2^+ bond cleavage propensity, among others. A photo-induced borylation reaction was then investigated with all the photosensitizers and proceeded with yields between 9% and 74%.

INTRODUCTION

Diazonium salts, first prepared by Peter Griess in the late 1850s,[1] represent a well-known class of reactive molecules that have always attracted much attention because of their interesting chemistry as well as ease of preparation.[2] Indeed, diazotization is simply performed by reacting the parent aniline with a nitroso group, either formed *in situ* via the reaction of $NaNO_2$ with HCl for example, or via commercial derivatives such as ^tBuONO or $NOBF_4$. The main drawback of aryl diazonium derivatives is their lack of thermal stability, which can result in more challenging handling. Stability is usually increased when diazonium derivatives are isolated as tetrafluoroborate salts.

Despite this, diazonium salts have found numerous applications, and probably the most widespread one is in the dyeing industry, as the azo-coupling reactions often yield intensely colored pigments. Organic chemists have taken an interest in the ease with which the N_2 group can be displaced, and this displacement was historically used in the Sandmeyer, Pschorr, Gomberg-Bachmann, Meerwein, or Balz-Schiemann reactions and is nowadays commonly used in (transition metal catalyzed) aryl C–C and aryl C–heteroatom bond formation.[2] With the exception of the Balz-Schiemann reaction, which occurs via thermal or light activation, these historic reactions proceed via the exogenous reduction of aryl diazonium salts using a (sacrificial) electron donor, where the chemical reduction generates the corresponding reactive aryl radical and the inert N_2 gas. The resulting radical can then be used to drive a

THE BIGGER PICTURE

Factors controlling excited-state reactivity are of paramount importance, as a better understanding of these would yield more efficient photo-induced processes. This is relevant not only for photoredox catalysis but also for all fields that use light to trigger reactions, which include—but are not limited to—photochemotherapy and solar fuel formation such as water oxidation, halide oxidation, and proton or carbon dioxide reduction. Here, we investigated reactions between a large series of Ru(II), Os(II), Ir(III), Cu(I), and Fe(III) photosensitizers and 13 diazonium salts, which included macrocyclic derivatives. Clear explanations of dark and excited-state reactivity are provided. The efficiencies of formation of charge-separated products (also termed cage-escape yields) generating radical species of paramount importance for additional targeted transformation were quantified in different media and with varying driving force for electron transfer.

Please cite this article in press as: Ripak et al., Photosensitized activation of diazonium derivatives for C–B bond formation, Chem Catalysis (2022), https://doi.org/10.1016/j.checat.2022.100490

plethora of organic chemistry transformation.[2–7] Alternatively, the radicals can also be used for surface modification of conducting, semi-conducting, and insulating surfaces as well as nanoparticles, as pioneered by Pinson et al. in the 1990s.[6,8–11]

Aryl diazonium salts are also very versatile reagents in photoredox catalysis, where they can be reduced via excited-state electron transfer from a photosensitizer (PS). In 1984, Cano-Yelo and Deronzier reported one of the first visible-light-activated Pschorr reactions using the prototypical $[Ru(bpy)_3]^{2+}$ PS.[12,13] In this example, the photochemical approach led to intramolecular cyclization with 100% yield, whereas the thermal dark pathway led to lower yields and isomeric side-products. This reaction sparked a renewed interest in photo-redox catalysis and its use toward the activation of aryl diazonium derivatives.

The photophysical scheme governing the photoreaction, including the different steps relevant for the present study, is presented in Scheme 1. Photon absorption by the PS leads to the formation of an excited state (PS*) that can diffuse to generate an encounter complex with the quencher, 4-MeO-benzene diazonium in this case. A geminate radical pair composed of the oxidized PS ($PS^{\bullet+}$) and the reduced diazonium moiety is then formed if the driving force for electron transfer is favorable. This geminate radical pair can either undergo geminate charge recombination (k_{GCR}) to form the initial reactants or, more interestingly for the field of photoredox catalysis, undergo cage escape (φ_{CE}) to generate the separated, charged species (Scheme 1). The solvent separated radicals can either undergo back-electron transfer (k_{BET}) or bond dissociation of the reduced diazonium can occur, freeing the inert N_2 gas and the reactive aryl radical for further reactivity. Often mentioned in the literature is the regeneration of the ground-state photosensitizer via oxidation of an organic intermediate at a given stage within the reaction scheme ($PS^{\bullet+}$ to PS in Scheme 1).

Numerous examples of the use of aryl diazonium in photoredox catalysis have since emerged. König et al. used these substrates for the direct C–H arylation of furan, thiophene, and Boc-protected pyrrole scaffolds.[14] Tlili et al. also recently reported the conversion of aryl diazonium salts into arylsulfonyl fluorides using DABSO, KHF_2, and a cyanoarene PS (3DPAFIPN).[15] Sandford et al. reported the ligand-directed C–H arylation reaction using aryl diazonium salts through the merger of palladium-catalyzed C–H functionalization and visible-light photoredox catalysis with a $[Ru(bpy)_3]^{2+}$ PS.[16] Finally, Yan et al. used Eosin Y as PS for the visible-light-induced borylation of aryldiazonium salts.[17] Several reviews are dedicated to the (photo)chemical reduction of aryl diazoniums for organic chemistry and surface modification.[2–7]

In light of the widespread applicability of photosensitized aryl diazonium activation, we became interested in understanding key factors that govern their excited-state reactivity, product separation after electron transfer, and N_2 dissociation (Scheme 1). To reach that goal, a series of nine rare and earth-abundant transition metal PSs were selected. This permitted tuning of ground- and excited-state redox properties, nature of excited-state transitions, as well as modulation of the visible absorption range. We investigated their excited-state reactivity with a series of 13 aryl diazonium salts, which included three macrocyclic calix[4]arene tetradiazonium derivatives,[4,11] using a variety of steady-state and time-resolved spectroscopic techniques. The emphasis was placed on determining mechanistically relevant information that would be useful for the future design of catalytic photoredox transformations.

[1]Université Catholique de Louvain (UCLouvain), Institut de la Matière Condensée et des Nanosciences (IMCN), Molecular Chemistry, Materials and Catalysis (MOST), Place Louis Pasteur 1, bte L4.01.02, 1348 Louvain-la-Neuve, Belgium

[2]Department of Chemistry, University of North Carolina at Chapel Hill, Chapel Hill, NC 27599-3290, USA

[3]Department of Biochemistry, The University of Texas Southwestern Medical Center, 5323 Harry Hines Boulevard, Dallas, TX 75390-9038, USA

[4]Spectroscopy, Quantum Chemistry and Atmospheric Remote Sensing (CP 160/09), Université Libre de Bruxelles (ULB), 50 av. F. D. Roosevelt, CP160/09, 1050 Brussels, Belgium

[5]Laboratoire de Chimie Organique, Université Libre de Bruxelles (ULB), Avenue F. D. Roosevelt 50, CP160/06, 1050 Brussels, Belgium

[6]Lead contact

*Correspondence: ludovic.troian@uclouvain.be

https://doi.org/10.1016/j.checat.2022.100490

Please cite this article in press as: Ripak et al., Photosensitized activation of diazonium derivatives for C–B bond formation, Chem Catalysis (2022), https://doi.org/10.1016/j.checat.2022.100490

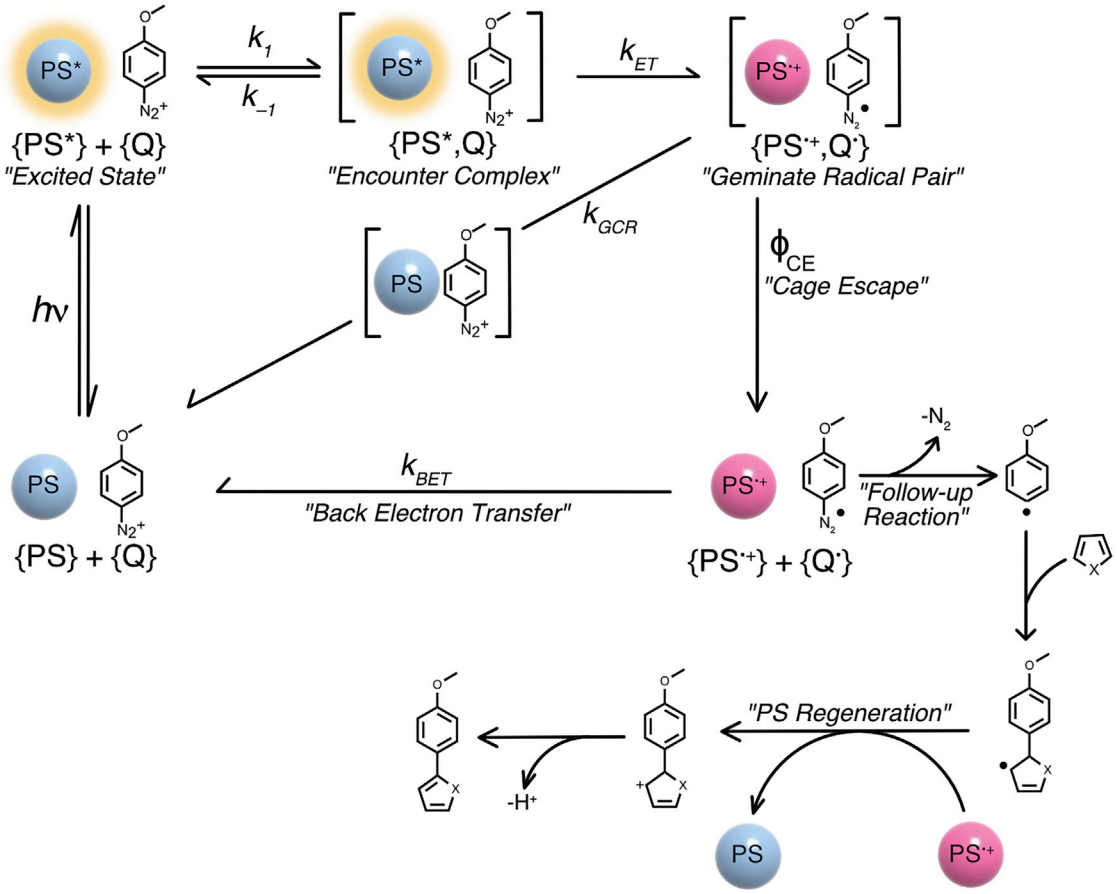

Scheme 1. Photophysical and photochemical scheme describing the reaction between a PS and 4-MeO-benzene diazonium (Q) under irradiation
The successive reaction is a representative example reported by König et al.[14]

RESULTS AND DISCUSSION

Synthesis

Figure 1 displays the structure of the nine PSs as well as the ten aryl diazonium and three calix[4]arene tetradiazonium derivatives included in this study. Most of the PSs were either commercially available or were synthesized via reported procedures.[18–20] $[Fe(Br\text{-}phtmeimb)_2]^+$, where Br-phtmeimb is tris(3-methylimidazolium-1-yl)(4-Br-phenyl)borate, was synthesized by reacting $FeBr_2$ and Br-phtmeimb in anhydrous THF at room temperature for 48 h. Wärnmark et al. very recently reported the synthesis of $[Fe(Br\text{-}phtmeimb)_2]^+$, which occurred with similar yields but in much shorter reaction times in anhydrous DMF.[21] Br-phtmeimb was synthesized in two steps starting from (4-bromophenyl)-trimethylsilane that first underwent reaction with BBr_3 in dichloromethane at −78°C following a related procedure reported by Kaufmann in 1987.[22] The resulting 4-bromo-dibromophenylborane was directly reacted with imidazole in toluene in the presence of TMSCl, similarly to the procedure reported by Smith et al.[23] The use of TMSCl allowed for easier recovery of tris(3-methylimidazolium-1-yl)(4-Br-phenyl)borate in 80% yield over two steps after ion metathesis using ammonium hexafluorophosphate in water. The different diazonium derivatives were either commercially available or were synthesized by reaction of the parent aniline with $NOBF_4$ in acetonitrile at −40°C for 2 h.[10,24] The diazonium salts were obtained in almost quantitative yields following several washing steps. As depicted in Figure 1, the aryl diazonium salts were *para* substituted with several electron

Please cite this article in press as: Ripak et al., Photosensitized activation of diazonium derivatives for C–B bond formation, Chem Catalysis (2022), https://doi.org/10.1016/j.checat.2022.100490

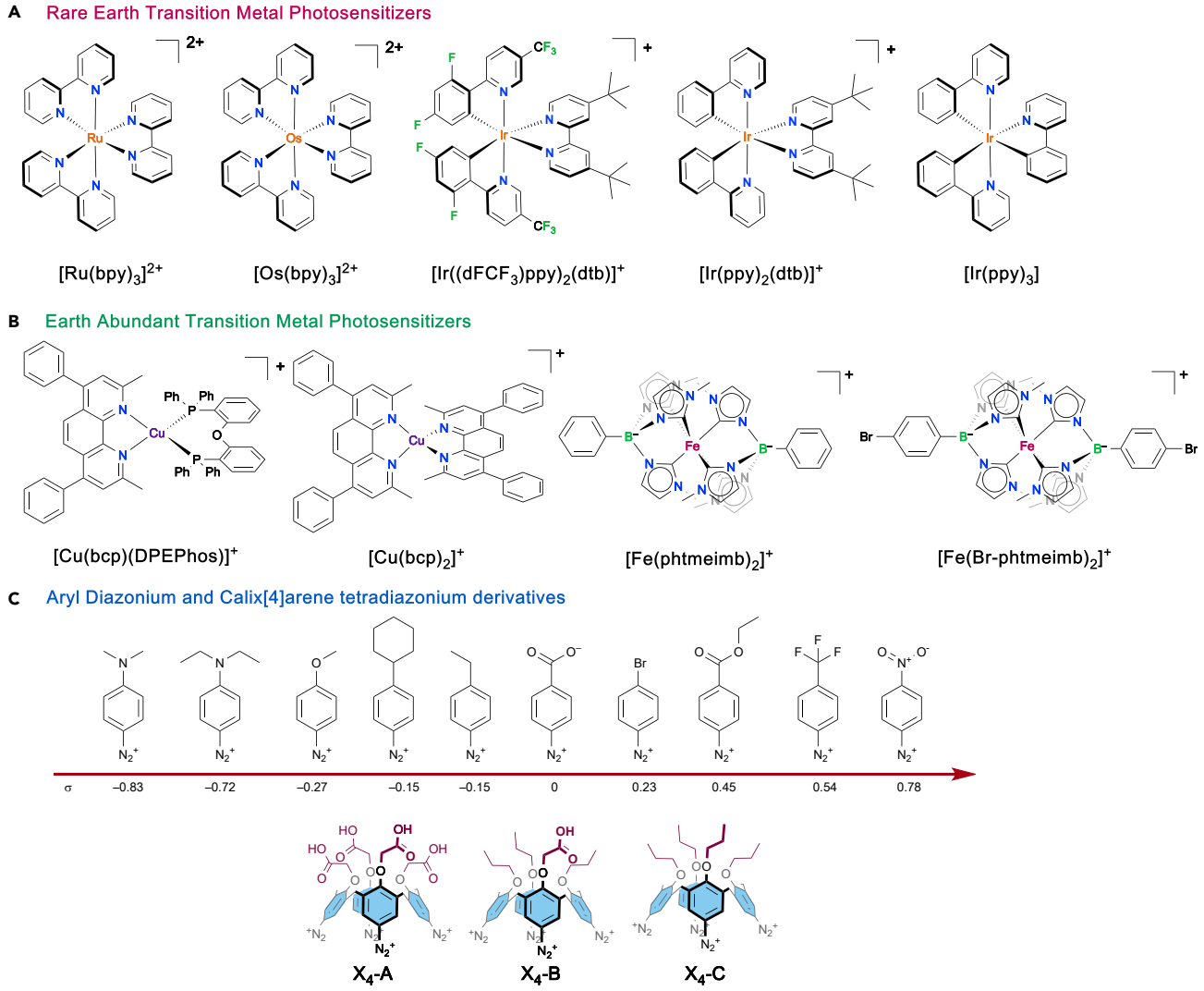

Figure 1. Structures of the PSs and aryl diazonium derivatives

Structures of the different rare (A) and earth-abundant (B) PSs isolated as hexafluorophosphate salts (when charged) as well as (C) the calix[4]arene tetradiazonium and aryl diazonium salts investigated herein, including their respective Hammett parameter (σ). All overall positively charged diazonium derivatives had tetrafluoroborate counter ion(s).

donating/withdrawing groups that permitted tuning of the Hammett parameter (σ) from −0.83 for 4-(N,N)-diethylamine benzene diazonium tetrafluoroborate to 0.78 for the 4-nitrobenzene diazonium tetrafluoroborate analogue.[25] The calix[4]arene tetradiazonium derivatives are particularly interesting substrates as they represent polydiazonium compounds that have not been investigated thus far for excited-state quenching applications. In addition, tetrasubstituted calix[4]arenes represent a very important class of macrocyclic compounds, and developing strategies to poly-functionalize these macrocycle is therefore essential.[4,26] The possibility to trigger light-activated processes using these compounds could in the future lead to a new class of synthetic approaches toward these macrocyclic derivatives.

Ground- and excited-state properties

The ground-state absorption spectra of the different PSs were recorded in argon-purged acetonitrile at room temperature (Figure 2). The three Ir(III) PSs exhibited

Please cite this article in press as: Ripak et al., Photosensitized activation of diazonium derivatives for C–B bond formation, Chem Catalysis (2022), https://doi.org/10.1016/j.checat.2022.100490

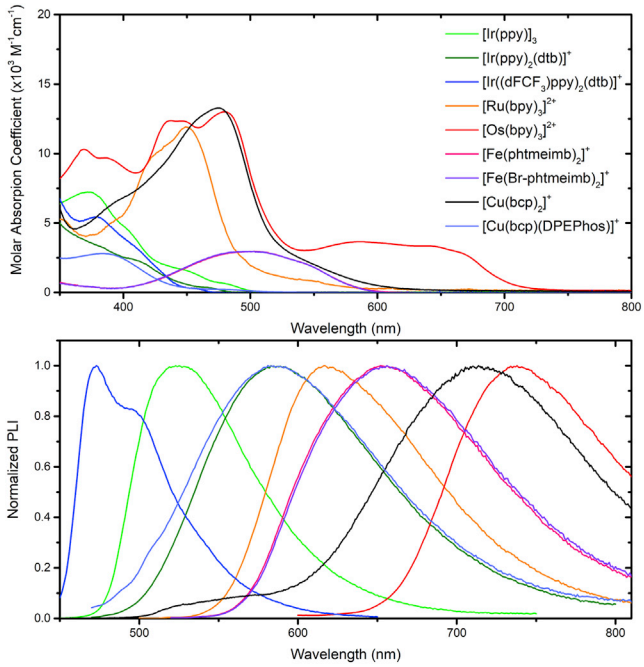

Figure 2. Absorption and PL spectra

of $[Ir(ppy)_3]$ (green), $[Ir(ppy)_2(dtb)]^+$ (dark green), $[Ir((dFCF_3)ppy)_2(dtb)]^+$ (blue), $[Ru(bpy)_3]^{2+}$ (orange), $[Os(bpy)_3]^{2+}$ (red), $[Fe(phtmeimb)_2]^+$ (pink), $[Fe(Br\text{-}phtmeimb)_2]^+$ (violet), $[Cu(bcp)_2]^+$ (black, recorded in dichloromethane), and $[Cu(bcp)(DPEPhos)]^+$ (light blue) recorded at room temperature in argon-purged acetonitrile.

moderate absorption features at wavelengths greater than 400 nm, and $[Ru(bpy)_3]^{2+}$ exhibited the classical singlet metal-to-ligand charge transfer (^{1}MLCT) band around 450 nm with molar absorption coefficient of 12,000 $M^{-1}cm^{-1}$.[27–29] Similar ^{1}MLCT transitions were observed for $[Os(bpy)_3]^{2+}$ with a slightly larger molar absorption coefficient. In addition, direct ^{3}MLCT excitation at wavelengths greater than 550 nm were also observed due to the larger spin-orbit coupling conferred by the heavier Os(II) center.[27,30] The heteroleptic $[Cu(bcp)(DPEPhos)]^+$ absorbed very weakly in the visible region, whereas $[Cu(bcp)_2]^+$ exhibited intense ^{1}MLCT transitions with molar absorption coefficients around 13,000 $M^{-1}cm^{-1}$ at 480 nm.[31–34] Finally, both Fe(III) PSs exhibited a doublet ligand-to-metal charge transfer band at 500 nm with a molar absorption coefficient of 2,950 $M^{-1}cm^{-1}$.[20,21] The introduction of Br groups had no significant impact on the UV-visible (UV-vis) absorption features.

Excitation of the different PSs in acetonitrile within the visible range of the solar spectrum led to room temperature (PL) that ranged from 472 nm for $[Ir((dFCF_3)ppy)_2(dtb)]^+$ to 737 nm for $[Os(bpy)_3]^{2+}$. Note that the emission of $[Cu(bcp)_2]^+$ was extremely weak in acetonitrile under argon and was thus recorded in dichloromethane. Time-resolved measurements of the PL in argon-purged acetonitrile containing 0.1 M $TBABF_4$ were well described by first-order kinetics, which yielded excited-state lifetimes ranging from 2 to 2010 ns (Table 1). The decision to perform measurements in 0.1 M $TBABF_4$ was motivated by the desire to work at fixed ionic strength to avoid further salt effects that could have originated upon the titration of aryl diazonium tetrafluoroborate derivatives (*vide infra*). For $[Fe(phtmeimb)_2]^+$ and $[Fe(Br\text{-}phtmeimb)_2]^+$, the excited-state lifetimes were obtained through reconvolution of the instrument response function (IRF) and a simulated single-exponential function to model the measured decay in signal (Figures S88–S95).

Please cite this article in press as: Ripak et al., Photosensitized activation of diazonium derivatives for C–B bond formation, Chem Catalysis (2022), https://doi.org/10.1016/j.checat.2022.100490

Table 1. Excited-state lifetimes of the nine PSs in different media

	CH_3CN		CH_3CN + 0.1 M $TBABF_4$	
PS	τ (ns)[a]	τ (ns)[b]	τ (ns)[a]	τ (ns)[b]
$[Ru(bpy)_3]^{2+}$	193	850	165	890
$[Os(bpy)_3]^{2+}$	39	57	37	55
$[Ir((dFCF_3)ppy)_2(dtb)]^+$	157	2,010	142	1,890
$[Ir(ppy)_2(dtb)]^+$	63	554	64	543
$[Cu(bcp)(DPEPhos)]^+$	120	1,100	153	1,050
$[Cu(bcp)_2]^+$[c]	50	58	34	35
$[Fe(Br\text{-}phtmeimb)_2]^+$	2	2	2	2
$[Fe(phtmeimb)_2]^+$	2	2	2	2
$[Ir(ppy)_3]$	45	1,400	24	1,420

[a]Recorded under air.
[b]Recorded under argon.
[c]Recorded in dichloromethane.

This yielded an excited-state lifetime of 2 ns for $[Fe(phtmeimb)]^+$ as well as for $[Fe(Br\text{-}phtmeimb)]^+$, in agreement with literature values.[20,21]

Cyclic voltammetry and differential pulse voltammetry (DPV) allowed determination of the reduction potentials of the different aryl diazoniums and PSs. In Table 2, the PSs are sorted according to their excited-state oxidation potential E_{ox}*; i.e., according to their ability to release one electron from their excited state. The energy stored in the excited state (E_{00}) was estimated using the generalizable method of extrapolating a tangent line on the blue edge of the corrected PL spectrum to the emission baseline.[35–37] The excited-state redox potentials were then determined using E_{00} and the following equations:

$$E^*_{red} = E_{red} + E_{00} \quad \text{(Equation 1a)}$$

$$E^*_{ox} = E_{ox} - E_{00} \quad \text{(Equation 1b)}$$

The values obtained from these equations matched those reported in the literature.[20,21,31,38–40] $[Ru(bpy)_3]^{2+}$, $[Os(bpy)_3]^{2+}$, $[Ir((dFCF_3)ppy)_2(dtb)]^+$, $[Ir(ppy)_2(dtb)]^+$, and $[Cu(bcp)(DPEPhos)]^+$ exhibit similar excited-state oxidation potentials ranging from −0.63 to −0.78 V versus NHE. The largest difference between those PSs stems from the ground-state oxidation potentials, which range from 1.02 V versus NHE for $[Os(bpy)_3]^{2+}$ to +1.93 V versus NHE for $[Ir((dFCF_3)ppy)_2(dtb)]^+$. $[Ir(ppy)_3]$, $[Fe(phtmeimb)_2]^+$, and $[Fe(Br\text{-}phtmeimb)_2]^+$ are the strongest reductants in their excited state, with E_{ox}* of −1.49, −1.29, and −1.23 V versus NHE, respectively. They exhibit ground-state oxidation potentials of +1.01, +0.85, and +0.91 V versus NHE for $[Ir(ppy)_3]$, $[Fe(phtmeimb)_2]^+$, and $[Fe(Br\text{-}phtmeimb)_2]^+$, respectively.

The aryl diazonium reduction waves were irreversible, and the corresponding potentials were estimated by DPV. Reduction potentials ranged from −0.51 to 0.77 V versus NHE and trended linearly with their Hammett parameters (Figure 3A).

Excited-state quenching

The electrochemical data and the excited-state redox properties suggested that excited-state electron transfer from the PSs to the aryl diazonium derivatives would be in all cases thermodynamically favorable as diazonium derivatives possess reduction potentials in the −0.5 to +0.8 V versus NHE range. Hence, time-resolved Stern-Volmer titration were carried out with all PSs, with the exception of both Fe(III) PSs

Please cite this article in press as: Ripak et al., Photosensitized activation of diazonium derivatives for C–B bond formation, Chem Catalysis (2022), https://doi.org/10.1016/j.checat.2022.100490

CellPress

Table 2. Electrochemical properties of the nine PSs

	Ground state		Excited state	
PS	E_{ox}[a,b]	E_{red}[a,b]	E_{ox}*[b]	E_{red}*[b]
$[Ru(bpy)_3]^{2+}$	+1.50	−1.11	−0.63	+1.02
$[Os(bpy)_3]^{2+}$	+1.02	−1.06	−0.65	+0.61
$[Ir((dFCF_3)ppy)_2(dtb)]^+$	+1.93	−1.13	−0.65	+1.45
$[Ir(ppy)_2(dtb)]^+$	+1.45	−1.27	−0.72	+0.90
$[Cu(bcp)(DPEPhos)]^+$	+1.49	−1.40	−0.78	+0.87
$[Cu(bcp)_2]^+$	+0.92	−1.38	−1.05	+0.59
$[Fe(Br\text{-}phtmeimb)_2]^+$	+0.91	−0.51	−1.23	+1.58
$[Fe(phtmeimb)_2]^+$	+0.85	−0.56	−1.29	+1.63
$[Ir(ppy)_3]$	+1.01	−1.95	−1.49	+0.55

[a]Recorded in CH_3CN containing 0.1 M $TBAPF_6$.
[b]In V versus NHE.

that were instead investigated via steady-state PL quenching experiments. Both copper complexes were also studied but showed lack of stability and are hence not presented herein. All steady-state and time-resolved quenching experiments were carried out in argon-purged acetonitrile containing 0.1 M $TBABF_4$. The lifetime of the PSs in acetonitrile and acetonitrile containing 0.1 M $TBABF_4$ are reported in Table 1. We chose to work at fixed ionic strength to avoid salt effects that could have originated upon the titration of aryl diazonium tetrafluoroborate derivatives. A representative example of the excited-state quenching of $[Ir(ppy)_3]$ with 4-MeO-benzene diazonium is presented in Figure 3B. In almost all cases, the gradual increase of quencher concentration led to appreciable quenching of the PS's excited-state lifetime (Figures S1–S66). In some cases, additional static quenching was observed by a decrease of the initial time-resolved PL amplitude. The quenching rate constants (k_q) obtained with $[Ru(bpy)_3]^{2+}$, $[Os(bpy)_3]^{2+}$, $[Ir((dFCF_3)ppy)_2(dtb)]^+$, $[Ir(ppy)_2(dtb)]^+$, and $[Ir(ppy)_3]$ with all the diazonium derivatives were in the (1.08–25.1) × 10^9 $M^{-1}s^{-1}$ range (i.e., close to the solvent diffusion limit). These values are compiled in Table 3. These quenching rate constants increased with the driving force for electron transfer (Figure 3D), before reaching a plateau when $[Ir(ppy)_3]$, the PS with the highest excited-state oxidation potential, was used. This plateau was reached at a driving force of around $-\Delta G_{ET} = \sim 1.2$ eV, which is in line with or slightly larger than the ~1 eV commonly observed in the literature for other systems.[41–45] Interestingly, the quenching rate constants also trended with Hammett parameters (Figure 3C). In all cases, a similar slope afforded reasonable fits of the data. The calix[4]arene tetradiazonium derivatives exhibited quenching rate constants that were slightly larger than the other ether derivatives (i.e., 4-MeO-benzene diazonium). This probably originates from the fact that the concentration of quencher, i.e., calix[4]arene, is taken into consideration when determining the quenching rate constant, and not the concentration of diazonium unit. In addition, most Stern-Volmer plots with calix[4]arenre tetradiazonium moiety exhibited downward curvature at higher concentrations. The reasons for such downward curvature are still unknown but could stem from changes in concentration of quencher during the experiments or from possible intramolecular side-reactions upon reduction.

Unfortunately, neither copper complexes remained stable enough in 0.1 M $TBABF_4$ CH_3CN solution during the experiment to afford unambiguous quenching rate constants. This was in line with the well-established heteroleptic to homoleptic conversion[46,47] via a ligand association-dissociation mechanism that occurs more rapidly in coordinating solvents, such as acetonitrile,[48] than in non-coordinating ones such as

Please cite this article in press as: Ripak et al., Photosensitized activation of diazonium derivatives for C–B bond formation, Chem Catalysis (2022), https://doi.org/10.1016/j.checat.2022.100490

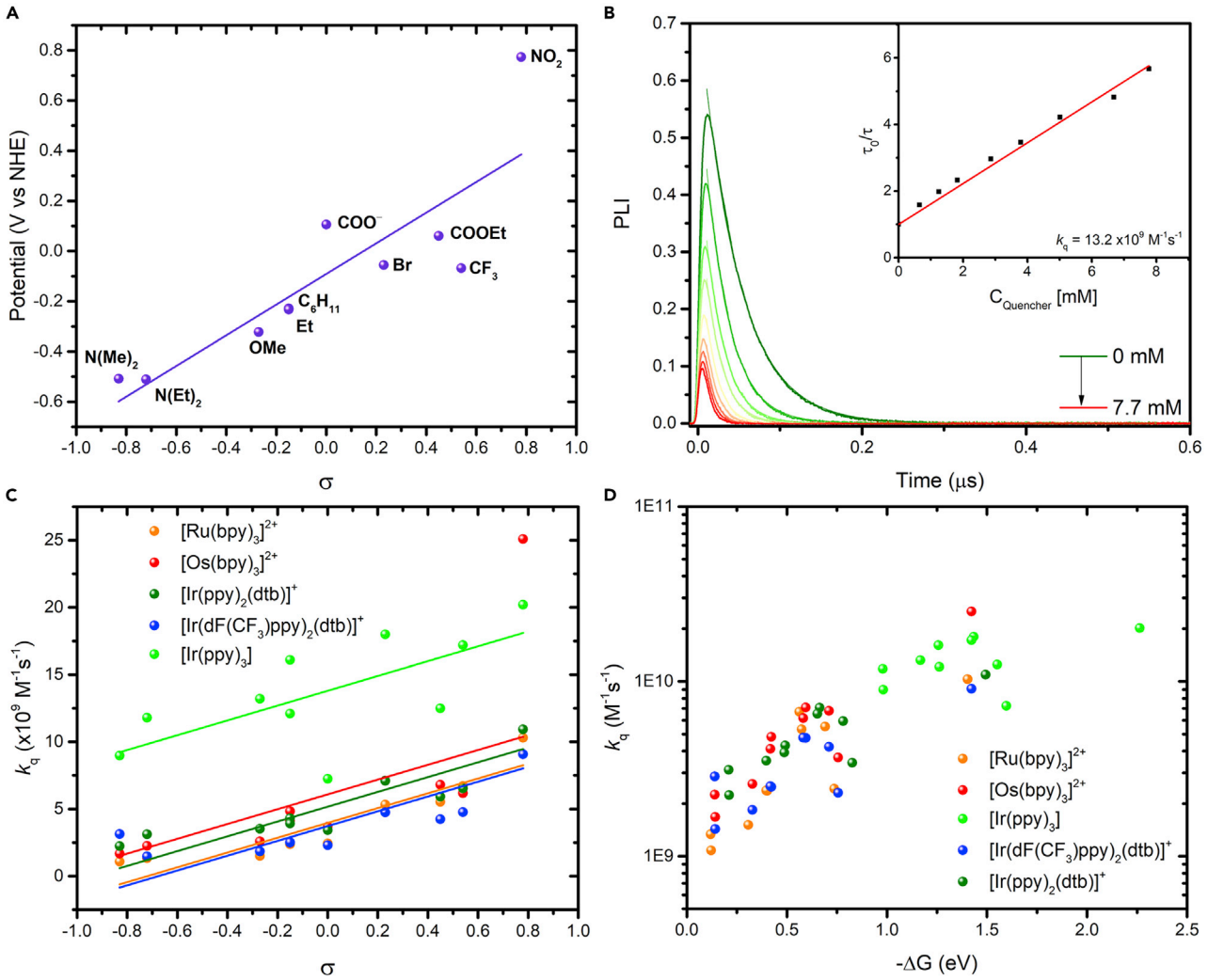

Figure 3. Electrochemical and excited-state characterization

(A) Reduction potential of the aryl diazonium as a function of Hammett parameters (σ) recorded in 0.1 M $TBAPF_6$ CH_3CN electrolyte at room temperature.

(B) Time-resolved PL quenching experiments and Stern-Volmer plot (inset) of $[Ir(ppy)]_3$ with increased concentration of 4-MeO-benzene diazonium. Experiments were carried out under argon in 0.1 M $TBABF_4$ CH_3CN solutions.

(C) Bimolecular quenching rate constants (k_q) as a function of Hammett parameters (σ) and (D) as a function of driving force (ΔG), for $[Ir(ppy)_3]$ (green), $[Ir(ppy)_2(dtb)]^+$ (dark green), $[Ir((dFCF_3)ppy)_2(dtb)]^+$ (blue), $[Ru(bpy)_3]^{2+}$ (orange), and $[Os(bpy)_3]^{2+}$ (red).

dichloromethane.[49] This process was also shown to occur upon oxidation of Cu(I) to Cu(II), either electrochemically[50] or under illumination.[51,52] Surprisingly, despite a large driving force for electron transfer, the Fe(III) complexes did not exhibit appreciable excited-state quenching (Figures S65 and S66). The possibility to perform excited-state oxidative quenching of $[Fe(phtmeimb)_2]^+$ was already realized by Wärnmark and coworkers using methylviologen with concentrations ranging from 10 to 500 mM.[20] We observed similar results when methylviologen was used with $[Fe(phtmeimb)_2]^+$ or $[Fe(Br\text{-}phtmeimb)_2]^+$, with k_q of 1.8×10^9 and $1.6 \times 10^9\ M^{-1}s^{-1}$, respectively. We were unable to increase the concentration range of 4-MeO-benzenediazonium to reach those used for the quenching by methylviologen, as dark reactivity was observed concomitantly, as will be further described (*vide infra*).

Please cite this article in press as: Ripak et al., Photosensitized activation of diazonium derivatives for C–B bond formation, Chem Catalysis (2022), https://doi.org/10.1016/j.checat.2022.100490

Table 3. Quenching rate constant (k_q) and numerical value of Hammett parameters (σ) for the indicated PS/aryl diazonium combinations

Diazonium (σ)	$[Ru(bpy)_3]^{2+}$[a]	$[Os(bpy)_3]^{2+}$[a]	$[Ir(ppy)_3]$[a]	$[Ir((dFCF_3)ppy)_2(dtb)]^{+}$[a]	$[Ir(ppy)_2(dtb)]^{+}$[a]
NMe_2 (−0.83)	1.08	1.67	8.97	1.43	2.25
NEt_2 (−0.72)	1.34	2.25	11.8	2.86	3.11
MeO (−0.27)	1.51	2.59	13.2	1.84	3.52
C_6H_{11} (−0.15)	2.37	4.83	12.1	2.49	4.32
Et (−0.15)	2.37	4.12	16.1	2.52	3.93
COO^- (0)	2.43	3.67	7.24	2.30	3.42
Br (0.23)	5.33	7.11	17.9	4.74	7.06
COOEt (0.45)	5.52	6.08	12.5	4.24	5.92
CF_3 (0.54)	6.71	6.17	17.2	4.78	6.53
NO_2 (0.78)	10.3	25.1	20.2	9.07	10.9
X_4-A	4.37	10.8	20.5	5.59	10.3
X_4-B	4.37	7.30	11.5	3.18	8.68
X_4-C	5.70	10.2	16.7	5.12	10.0

[a] k_q ($\times 10^9$ $M^{-1}s^{-1}$). Experiments were carried out at room temperature in argon-purged acetonitrile containing 0.1 M $TBABF_4$ electrolyte.

Photolysis

The quenching rate constants highlight that the five rare earth transition metal complexes were able to photo-react, supposedly via excited-state electron transfer, with all the aryl diazonium derivatives. Thermodynamically, all earth-abundant PSs should also be able to undergo excited-state reactivity with the diazonium. In an attempt to corroborate the excited-state reactivity, or lack thereof, and to further investigate the issue of photostability noted for the copper complexes, we performed photolysis experiments.[53] These were carried out with the different PSs in the presence of 30 mM 4-MeO-benzene diazonium in argon-purged acetonitrile. Three main pieces of information were expected from these photolysis experiments. The first one was to determine whether excited-state electron transfer can occur, even for the PSs for which excited-state quenching could not be monitored. This investigation is crucial for future transient absorption measurements as well as for photoredox catalytic measurements. The second one was the photostability of the PS in the ground and oxidized form in the presence of 30 mM 4-MeO-benzene diazonium. The third one was to obtain the molar absorption coefficient of the oxidized and reduced PSs. This is important for measurements of cage-escape yields (*vide infra*) that require Δε values.

A typical photolysis experiment is presented in Figure 4 with $[Os(bpy)_3]^{2+}$ and with $[Fe(phtmeimb)_2]^{+}$. Illumination of a solution of $[Os(bpy)_3]^{2+}$ with 30 mM 4-MeO-benzene diazonium led to the gradual bleach of the MLCT transitions within 10 min of continuous irradiation, indicative of the formation of Os(III). Ascorbic acid was then added to test reversibility, which allowed for the immediate recovery of the authentic $[Os(bpy)_3]^{2+}$ spectra. The slight difference observed between the original spectra and the one after the addition of ascorbic acid stems from a combination of the absorbance of reduced aromatic compounds that tails into the visible range as well as some scattering induced by the moderately soluble ascorbic acid. When $[Fe(phtmeimb)_2]^{+}$ was used, in conditions where no dark reactivity occurs (*vide infra*), illumination for 60 min led to the gradual bleach of the ^{2}LMCT transition accompanied by the concomitant growth of a broad absorbance centered around 700 nm. This band was previously attributed to the formation of Fe(IV) species.[20] The longer irradiation time probably stems from smaller quenching rate constant, lower cage-escape yields, or the fact that the excited-state electron transfer from

Please cite this article in press as: Ripak et al., Photosensitized activation of diazonium derivatives for C–B bond formation, Chem Catalysis (2022), https://doi.org/10.1016/j.checat.2022.100490

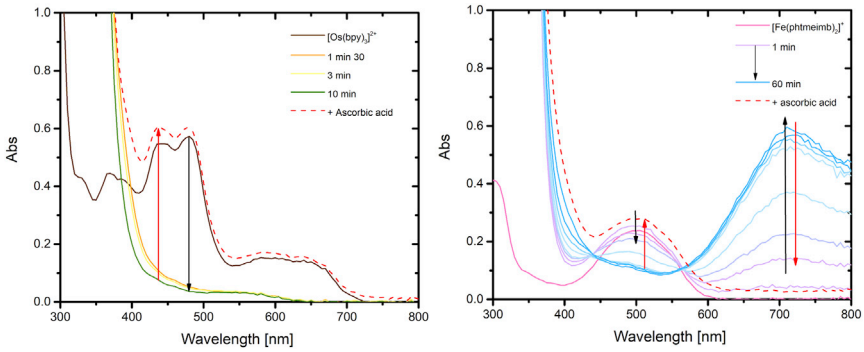

Figure 4. Photolysis experiments

Photolysis experiments of $[Os(bpy)_3]^{2+}$ (left) and $[Fe(phtmeimb)_2]^+$ (right) in argon-purged acetonitrile in the presence of 30 mM MeO-benzene diazonium. Reversibility was assessed through the addition of ascorbic acid at the end of the photolysis experiment (red dashed lines).

the iron-localized excited state to the diazonium could be kinetically slow. Nevertheless, the formation of Fe(IV) was also reversible, as observed by the recovery of the initial ^{2}LMCT transition upon the addition of ascorbic acid. Similar reactivity was observed for $[Fe(Br\text{-}phtmeimb)_2]^+$, which exhibited a molar absorption coefficient for the Fe(IV) form of 7,030 $M^{-1}cm^{-1}$ (Figure S75). Reversibility was also observed with $[Ru(bpy)_3]^{2+}$ (Figure S79). $[Ir(ppy)_3]$ seemed to exhibit some degree of irreversibility under these conditions (Figure S78), whereas, for the two other iridium complexes, the changes in absorption spectra upon photolysis were too small to unambiguously discuss reversibility (Figures S76 and S77). We also encountered partial reversibility for $[Cu(bcp)_2]^+$ (Figure S73) and observed the growth of a peak around 480 nm when $[Cu(bcp)(DPEPhos)]^+$ was used, consistent with the *in situ* formation of $[Cu(bcp)_2]^+$ upon illumination in these conditions, as already known in the literature for similar complexes (Figure S74).[48,54]

Dark reactivity

As mentioned before, reactivity in the dark was observed when $[Fe(phtmeimb)_2]^+$ or $[Fe(Br\text{-}phtmeimb)_2]^+$ was mixed with selected diazonium salts. For example, in a solution mixture containing 4-Br-benzene diazonium, the bright red color of $[Fe(phtmeimb)_2]^+$ gradually changed to a persistent blue, which was unambiguously attributed to the formation of Fe(IV). Also, when the more electron-deficient 4-NO_2-benzene diazonium was used as the oxidant, the Fe(IV/III) color change was almost instantaneous to the unaided eye. These qualitative observations were fully consistent with a ground-state thermal electron transfer, despite thermodynamic predictions suggesting a highly endergonic ΔG of 0.80 eV for electron transfer based on the one-electron reduction potentials; i.e., $E_{1/2}(Fe^{(IV/III)})$ = 0.85 V versus NHE and 4-Br-benzene diazonium reduction ($E_{1/2}(Br\text{-}N_2^{(+/\bullet)}) \approx$ 0.05 V versus NHE). When, instead, the more electron rich 4-MeO-benzene diazonium was used, the solution mixture maintained the Fe(III) red color for several hours, indicating that the thermal electron transfer was significantly inhibited in these experimental conditions.

The reaction sequence for the net activation of the diazonium substrates in the dark is described here by a consecutive irreversible chemical reaction with a reversible electron transfer step according to Equation 2.

$$Fe(III) + R - N_2^+ \underset{k_{-1}}{\overset{k_1}{\rightleftharpoons}} Fe(IV) + R^{\bullet}N_2 \overset{k_2}{\rightarrow} Fe(IV) + R^{\bullet} + N_2(g) \qquad \text{(Equation 2)}$$

Please cite this article in press as: Ripak et al., Photosensitized activation of diazonium derivatives for C–B bond formation, Chem Catalysis (2022), https://doi.org/10.1016/j.checat.2022.100490

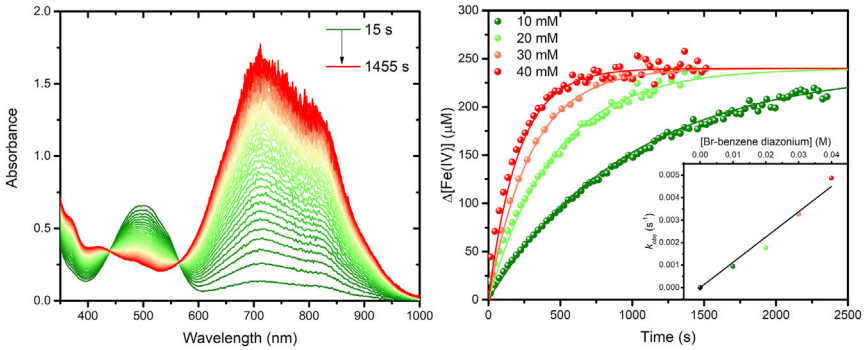

Figure 5. Dark reactivity of $[Fe(phtmeimb)_2]^+$ with 4-Br-benzene diazonium

Absorption changes (left) recorded in acetonitrile at selected time intervals for a solution of $[Fe(phtmeimb)_2]^+$ (230 μM) in the presence of 20 mM 4-Br-benzene diazonium. Absorption changes recorded at 700 nm (right) at different concentration of 4-Br-benzene diazonium. The inset shows the observed rate at each concentration that was used to determine the rate constant for electron transfer. This rate constant was used, in concert with Equations 2.1–2.3, to fit the absorption changes at 700 nm.

Quantitatively, Equation 2 is expressed by a set of coupled differential equations that describe the time-dependent concentration changes of all reactants and products,

$$\frac{d[Fe(III)]}{dt} = \frac{d[RN_2^+]}{dt} = -\frac{d[Fe(IV)]}{dt} = -k_1[Fe(III)][RN_2^+] + k_{-1}[Fe(IV)][R^{\bullet}N_2] \quad \text{(Equation 2.1)}$$

$$\frac{d[R^{\bullet}N_2]}{dt} = -k_2[R^{\bullet}N_2] - k_{-1}[Fe(IV)][R^{\bullet}N_2] \quad \text{(Equation 2.2)}$$

$$\frac{d[R^{\bullet}]}{dt} = k_2[R^{\bullet}N_2] \quad \text{(Equation 2.3)}$$

To test the proposed reaction pathway described by Equation 2, solution mixtures of 230 μM $[Fe(phtmeimb)_2]^+$ were prepared at various concentrations of Br-benzene diazonium, and the changes in absorption were monitored as a function of time. Kinetic traces monitored at 700 nm (Figure 5) or at 500 nm (Figure S110), which were representative of Fe(IV) formation, were analyzed by two different—but complementary—methods. First, by reasonably assuming $k_2 \gg k_1$, the kinetics of Equation 2 reduces to a single first-order kinetic reaction under the steady-state approximation, with k_1 being the rate-determining step. A linear fit of the observed rates plotted against the concentration of diazonium provided a rate constant k_1 of 0.115 $M^{-1}s^{-1}$ (Figure 5).

The kinetic traces in Figure 5 were then analyzed by numerically fitting the data to the set of differential equations using $k_1 = 0.115\ M^{-1}s^{-1}$ as a fixed input parameter. The reverse rate constant k_{-1} was substituted by the relationship $k_{-1} = k_1/K_{eq}$, where $K_{eq} = \exp(-\Delta G/RT)$ with $\Delta G = 0.80$ eV (at 298 K) as the initial guess. A global analysis of the kinetic traces in Figure 5 produced the best fits when $\Delta G = 0.66$ eV ($K_{eq} = 8 \times 10^{-12}$) and $k_2 \leq 1.0 \times 10^8\ s^{-1}$. Values for the dissociation constant of $R^{\bullet}N_2$ faster than 10 ns did not significantly improve the quality of the fit; in contrast, slower values of k_2 allow the reversible electron transfer, controlled by k_{-1}, to compete kinetically with the irreversible $R^{\bullet}N_2$ dissociation step. Using the value of $\Delta G = 0.66$ eV, and the Fe(IV/III) redox potential, the one-electron reduction potential for 4-Br-benzene diazonium was estimated at 0.19 V versus NHE. This value is about

Please cite this article in press as: Ripak et al., Photosensitized activation of diazonium derivatives for C–B bond formation, Chem Catalysis (2022), https://doi.org/10.1016/j.checat.2022.100490

0.14 V more positive than that estimated by DPV measurements, and naturally raised questions as to whether DPV or cyclic voltammetry methods provide accurate reduction potentials for irreversible reduction events, as observed for the series of benzene-substituted diazonium compounds.

In a pure reversible equilibrium, highly endergonic electron transfer reactions are often considered improbable when, in reality, a dynamic equilibrium exists where the concentrations of reactants and products are thermodynamically controlled by the balance of opposing forward and reverse rate constants, or the equilibrium constant. For reactions such as the one described by Equation 2, the presence of a fast and irreversible chemical step—the dissociation of $R^{\bullet}N_2$ that frees N_2—creates a reaction sink for the reversible electron transfer that shifts the product concentrations toward the right-hand side of Equation 2, in agreement with the Le Chatelier principle.

Transient absorption spectroscopy

Nanosecond transient absorption was then carried out to provide evidence that oxidative excited-state electron transfer was indeed occurring. First, the excited-state absorption spectra were recorded for the different PSs. Representative examples for $[Os(bpy)_3]^{2+}$ and $[Ir(ppy)_3]$ are shown in Figure 6, whereas the transient absorption spectra of $[Ru(bpy)_3]^{2+}$, $[Ir((dFCF_3)ppy)_2(dtb)]^{+}$, and $[Ir(ppy)_2(dtb)]^{+}$ are gathered in the supporting information (Figures S67–S72). The excited-state absorption spectra of $[Os(bpy)_3]^{2+}$ was typical for this class of PS; i.e., a ground-state bleach associated with the MLCT transitions, and positive absorption features below 410 nm and above 690 nm attributed to transition located on the reduced 2,2′-bipyridine following metal-to-ligand charge transfer. The transient absorption spectra, monitored at 490 nm, decayed with the same time constant as the one determined via time-resolved PL measurements. When similar experiments were carried out in the presence of 30 mM 4-MeO-benzene diazonium tetrafluoroborate, bleached signals were observed in almost the entire spectral window. The absence of positive absorption features coupled with the extremely long (greater than 300 μs) lifetime of the transient species are clear indicators of excited-state electron transfer and formation of the corresponding Os(III) center.

Similar results were obtained for $[Ir(ppy)_3]$ in argon-purged acetonitrile. The excited-state absorption spectra exhibited a bleach around 400 nm accompanied by positive absorption features below 370 nm and above 440 nm. Recovery of the ground-state bleach occurred with a similar rate as the one determined by time-resolved PL measurements. In the presence of 30 mM 4-MeO-benzene diazonium tetrafluoroborate, bleached signals were observed below 490 nm accompanied by positive absorption features above 490 nm. These spectral changes as well as the greater than 300-μs lifetime were also consistent with excited-state oxidation of $[Ir(ppy)_3]$. Similar observations were made with $[Ru(bpy)_3]^{2+}$, $[Ir((dFCF_3)ppy)_2(dtb)]^{+}$, and $[Ir(ppy)_2(dtb)]^{+}$ (Figures S67–S72). Transient absorption measurements were not attempted with the different copper complexes due to their previously noted lack of stability.

The results presented so far are in line with the accepted excited-state reaction scheme in solution that follows the undermentioned sequence: the excited PS diffuses toward the quencher (diazonium in this case), forming an "encounter complex" (Scheme 1). If thermodynamically favorable, the electron transfer event can occur, generating the corresponding geminate pair of radicals (oxidized and reduced species), $\{PS^{\bullet+};Q^{\bullet-}\}$. The latter was shown by Stern-Volmer experiments, photolysis, and nanosecond transient absorption spectroscopy. The geminate pair or radicals can

Please cite this article in press as: Ripak et al., Photosensitized activation of diazonium derivatives for C–B bond formation, Chem Catalysis (2022), https://doi.org/10.1016/j.checat.2022.100490

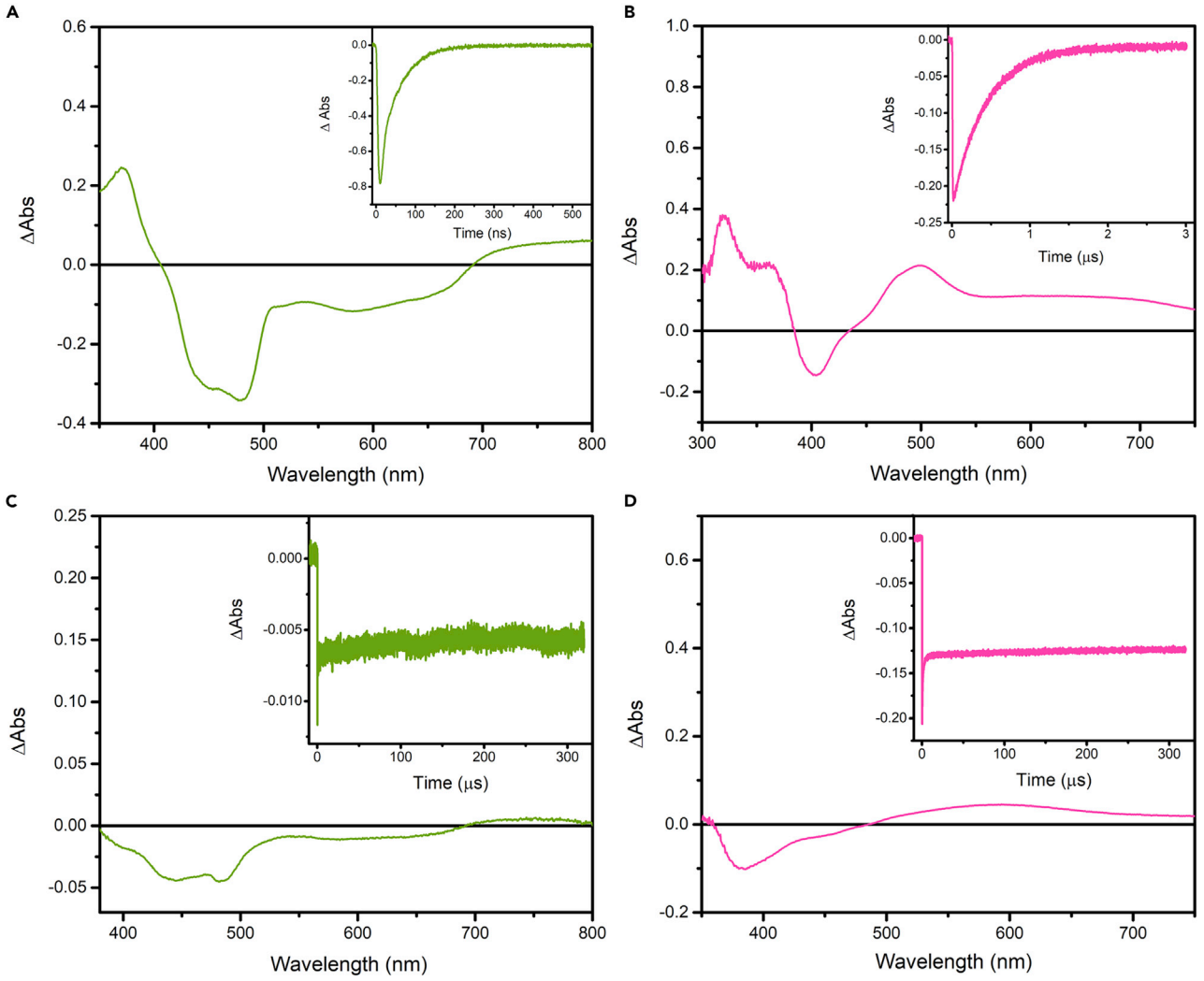

Figure 6. Excited-state characterization and reactivity of $[Os(bpy)_3]^{2+}$ and $[Ir(ppy)_3]$

(A and B) Nanosecond transient absorption spectra of $[Os(bpy)_3]^{2+}$ (A) and $[Ir(ppy)_3]$ (B) recorded 10 ns after the laser pulse (integrated for 50 ns) in argon-purged acetonitrile under argon atmosphere.

(C and D) Changes in absorption of $[Os(bpy)_3]^{2+}$ (C) and $[Ir(ppy)_3]$ (D) recorded 100 ns after the laser pulse (integrated for 100 ns) in the presence of 30 mM MeO-benzene diazonium. Insets represent the single-wavelength absorption changes recorded at 450 nm for $[Os(bpy)_3]^{2+}$ and 400 nm for $[Ir(ppy)_3]$, respectively. Experiments were carried out in argon-purged acetonitrile at room temperature. The sample were excited at 420 nm with a laser fluence of 10 mJ/pulse.

either recombine via geminate charge recombination to regenerate the initial state or undergo a cage-escape process to generate the charge-separated products that can be further used to drive additional organic transformations (Scheme 1). To date, there is no clear theory that allows prediction of the efficiency with which these oxidized and reduced species separate, yet it is of paramount importance for further improvement of light-driven applications.[19,41,55–58]

Cage-escape yields

The literature of cage-escape yields (φ_{CE}) for inorganic PS is mostly centered on $[Ru(bpy)_3]^{2+}$, which has often been considered as the prototypical inorganic PS. In a seminal paper, Olmsted and Meyer sought to understand the factors influencing φ_{CE}. To do so, they used methylviologen (MV^{2+}) as electron acceptor and a series

Please cite this article in press as: Ripak et al., Photosensitized activation of diazonium derivatives for C–B bond formation, Chem Catalysis (2022), https://doi.org/10.1016/j.checat.2022.100490

of Ru(II) and Os(II) PS, as well as some anthracene derivatives as electron donors. Olmsted and Meyer observed that φ_{CE} for the $\{M^{3+},MV^{\bullet+}\}$ pair varied only slightly within the series, with values that ranged from 14% to 27%.[59] However, when using an organic triplet as the electron donor, such as 9-methylanthracene or acridine yellow, φ_{CE} reached almost 100%. The yields dropped to 30% when perturbation by heavy atoms was introduced, as in the case of 9-bromoanthracene in solution containing CH_3I. The reported results highlighted that φ_{CE} were strongly affected by the rate of triplet-singlet interconversion of the triplet pair generated in the quenching event. In the absence of triplet-singlet mixing, as in the case of pure triplet organic donors, back-electron transfer, which requires a spin change, was slow compared with diffusion out of the solvent cage, which ultimately led to large φ_{CE}. When spin-orbit coupling was substantial, as with heavy-atom perturbators or in transition metal complexes, back-electron transfer became competitive with diffusional cage escape and thus led to lower φ_{CE}.

Kalyanasundaram and Neumann-Spallart later investigated the effects of added electrolyte on the φ_{CE} for the reaction between $[Ru(bpy)_3]^{2+*}$ and MV^{2+}. They found that φ_{CE} could vary by a factor of four upon changes in the nature of the medium by the addition of electrolytes. Experimentally, they determined that the quenching rate constant between the two doubly charged species increased as the ionic strength of the solution increased according to a "primary kinetic salt effect," as can be explained in terms of the Bronsted-Debye equation.[60] A φ_{CE} of 42% was determined in acetonitrile containing 0.1 M tetrabutylammonium perchlorate as electrolyte. This value decreased to 35% when 5% water was added to acetonitrile and reached 25% in neat or in buffered water at pH 4.7, in line with the results of Olmsted and Meyer.

We have recently attempted to understand factors influencing φ_{CE} using Fe(III) PS and to compare them with Ru(II) PS.[19,58] When triethylamine was used as electron donor, φ_{CE} for Ru(II) PS increased with solvent polarity: lower yields of 15% were found for CH_2Cl_2, moderate yields of 39% were found in CH_3CN, and much higher values were determined in DMF, φ_{CE} = 58%. This observation was in line with the expectation that polar solvents are better at stabilizing charged species. On the contrary, φ_{CE} values determined for the Fe(III) PS exhibited the opposite trend as those of Ru(II) PS; i.e., higher yields were measured in low-polarity solvents (φ_{CE} = 21% in CH_2Cl_2), whereas lower φ_{CE} were measured in DMF (φ_{CE} = 9%) and CH_3CN (negligible φ_{CE}).[40]

When Fe(III) PS was quenched by aniline derivatives, i.e., N,N-dimethyl-*p*-toluidine (DMT), dimethylaniline (DMA), or tritolylamine (TTA), φ_{CE} measured by comparative actinometry in DMF and CH_3CN were less than 7% but reached much higher values (between 36% and 63%) in CH_2Cl_2. This occurred despite very similar excited-state quenching rate constants in all three solvents. The low photo-product yields observed in CH_3CN were consistent with a report by Wärnmark et al., who determined φ_{CE} = 5% for both an N-phenylaniline electron donor and a methylviologen electron acceptor in CH_3CN.[20]

Our initial hypothesis that sparked this research project was that compounds such as aryl diazonium, which are known to be very reactive and irreversibly generate the inert N_2 gas upon one-electron reduction, would lead to increase cage-escape yields by impeding back-electron transfer within the solvent cage. The cage-escape yields (φ_{CE}) were determined for $[Os(bpy)_3]^{2+}$, $[Ru(bpy)_3]^{2+}$, $[Ir((dFCF_3)ppy)_2(dtb)]^{+}$, $[Ir(ppy)_2(dtb)]^{+}$, and $[Ir(ppy)_3]$ with a series of diazonium. These cage-escape yields were determined in neat CH_3CN as well as in the presence of 100 mM $TBABF_4$ for

Please cite this article in press as: Ripak et al., Photosensitized activation of diazonium derivatives for C–B bond formation, Chem Catalysis (2022), https://doi.org/10.1016/j.checat.2022.100490

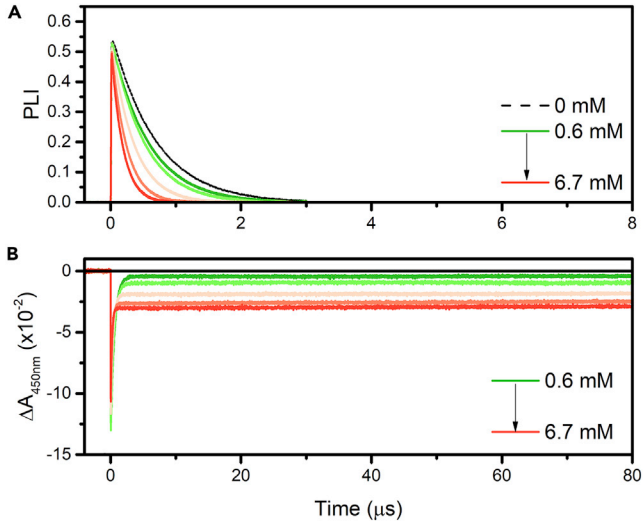

Figure 7. Representative dataset for $[Ru(bpy)_3]^{2+}$ quenched by 4-MeO-benzene diazonium in argon-purged acetonitrile at room temperature

(A) Excited-state lifetime at different concentration of 4-MeO-benzene diazonium used to determine the percentage of PL quenched.

(B) Changes in absorption recorded at 450 nm following pulsed light excitation at similar concentration of 4-MeO-benzene diazonium as in (A).

$[Ru(bpy)_3]^{2+}$. The cage-escape yields were determined by comparative actinometry using Equations 3 and 4 using $[Ru(bpy)_3]^{2+}$ as actinometer.[61] The maximum absorption changes generated from the oxidized PS (PS^+) were compared with the absorption maxima of the excited state of the reference $[Ru(bpy)_3]^{2+}$ (ES_{ref}) and normalized by their respective absorptances at the excitation wavelength (λ_{exc}). A $\Delta\varepsilon$ value of $-11{,}000\ M^{-1}cm^{-1}$ for the actinometer at 450 nm was used.[62–64] $\Delta\varepsilon_{450nm} = -9{,}000\ M^{-1}cm^{-1}$ and $\Delta\varepsilon_{470nm} = -12{,}000\ M^{-1}cm^{-1}$ were determined through the photolysis experiments for $[Ru(bpy)_3]^{2+}$ and $[Os(bpy)_3]^{2+}$, respectively, while $\Delta\varepsilon_{450nm} = 1{,}600\ M^{-1}cm^{-1}$ for $[Ir((dFCF_3)ppy)_2(dtb)]^+$ and $[Ir(ppy)_2(dtb)]^+$ was estimated following a modified reported procedure using transient absorption spectroscopy and MV^{2+} as electron acceptor.[65,66] The $\Delta\varepsilon_{450nm} = -9{,}000\ M^{-1}cm^{-1}$ was in line with the value obtained via spectroelectrochemistry, which enables us to confirm that, in this case, the photolysis approach allowed us to determine useful values of $\Delta\varepsilon$. A $\Delta\varepsilon_{530nm} = 1{,}700\ M^{-1}cm^{-1}$ for $[Ir(ppy)_3]$ was used based on reported spectroelectrochemical measurements.[67] Final cage-escape yield (φ_{CE}) values were obtained by comparing the relative yield of PS^+ produced (φ) with the percentage of quenched PL (%PL).

$$\Phi_{CE} = \frac{\Phi}{\%\ PL\ Quenched} \qquad \text{(Equation 3)}$$

$$\Phi = \left(\frac{\frac{\Delta A_{PS^+}}{\Delta\varepsilon_{PS^+}}}{\frac{\Delta A_{ES_{ref}}}{\Delta\varepsilon_{ES_{ref}}}}\right)\left(\frac{1 - 10^{-Abs_{ref}(\lambda_{exc})}}{1 - 10^{-Abs_{PS}(\lambda_{exc})}}\right) \qquad \text{(Equation 4)}$$

A representative example for $[Ru(bpy)_3]^{2+}$ with 4-MeO-benzene diazonium is represented in Figure 7.

The gradual increase of 4-MeO-benzene diazonium led to increased excited-state quenching, which was used to determine the percentage of PL quenched used in Equation 3. Each data point represents a freshly prepared sample with the indicated

Please cite this article in press as: Ripak et al., Photosensitized activation of diazonium derivatives for C–B bond formation, Chem Catalysis (2022), https://doi.org/10.1016/j.checat.2022.100490

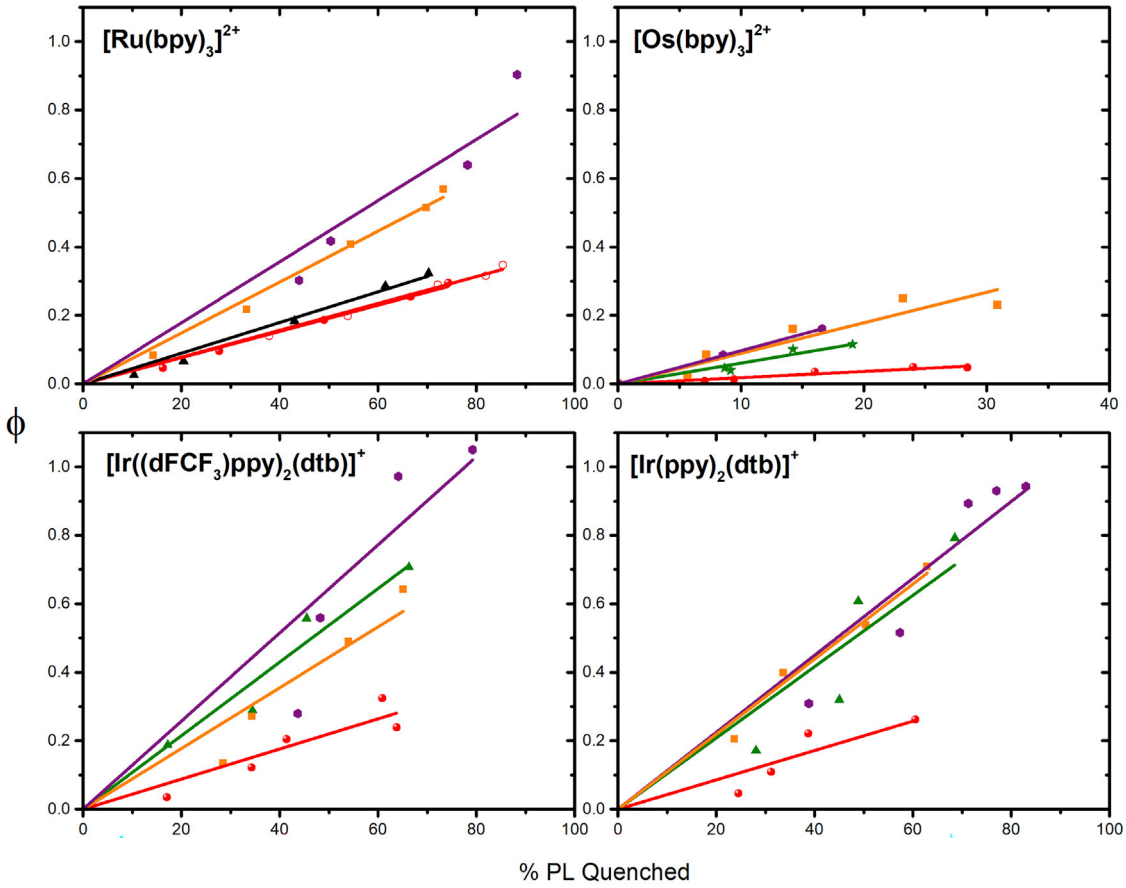

Figure 8. Relative yield of product versus the percentage of quenched PL

Plots of the relative yield of product (φ) versus the percentage of quenched PL (% PL quenched) for the indicated PSs in the presence of R-benzene diazonium, with R = MeO (red), ethyl (black), COOEt (orange), NO_2 (purple), and Br (green). Values recorded in 0.1 M $TBABF_4$ (for $[Ru(bpy)_3]^{2+}$) are represented with open red circles. The slope was used to extract the actual cage-escape yields, which are tabulated in Table 4.

concentration of aryl diazonium. The percentage of quenching was determined either via time-resolved PL or via steady-state PL when static quenching was observed. In parallel, the changes in absorption following pulsed light excitation are recorded at 450 nm. The value of ΔA recorded 10 μs after the laser pulse was used in Equation 4. Plots of φ versus the %PL quenched were all linear and the actual cage-escape values were extracted from the slope (Figure 8). The cage-escape yields are gathered in Table 4.

The cases of $[Ru(bpy)_3]^{2+}$ and $[Os(bpy)_3]^{2+}$ are the most straightforward to discuss. Indeed, the cage-escape yield increases from minimum values of 18% to maximum values of 98% when the driving force for electron transfer increases. The addition of 0.1 M $TBABF_4$ electrolyte did not affect the cage-escape yield when 4-MeO-benzene diazonium was used. In addition, these cage-escape yields also follow the $C–N_2^+$ bond cleavage propensity, as exemplified by the nuclear Fukui function (see below). For the iridium PSs, the cage-escape yield for 4-MeO-benzene diazonium was between 43% and 61% and reached values of 100% when the driving force was increased. The origin for the different cage-escape yields observed with a series of PSs using the same aryl diazonium is still unknown. Charge, electrostatic interactions, or dipole moment changes upon electron transfer might be responsible for these changes.

Please cite this article in press as: Ripak et al., Photosensitized activation of diazonium derivatives for C–B bond formation, Chem Catalysis (2022), https://doi.org/10.1016/j.checat.2022.100490

Table 4. Cage-escape yields (φ_{CE}) for the indicated PS/aryl diazonium combinations recorded in argon-purged acetonitrile

φ_{CE}	$[Ru(bpy)_3]^{2+}$[a]	$[Os(bpy)_3]^{2+}$	$[Ir(ppy)_3]$	$[Ir((dFCF_3)ppy)_2(dtb)]^+$	$[Ir(ppy)_2(dtb)]^+$
MeO (%)	38[b]	18	61	44	43
Br (%)	ND	61	100	100	100
COOEt (%)	74	89	ND	89	100
NO_2 (%)	98	97	ND	100	100

ND, not determined.

[a]A cage-escape yield of 45% was determined for $[Ru(bpy)_3]^{2+}$ using 4-ethylbenzene diazonium tetrafluoroborate.

[b]A value of 39% was determined in acetonitrile containing 0.1M $TBABF_4$. An error of 10% is assumed on each value.

Quantum mechanical calculations

Quantum mechanical calculations were used to investigate whether further correlations between the series of diazonium salts could be obtained. MP2 calculations[68–72] were first carried out using the 6-311G(d,p) basis set[73,74] with the Gaussian 16 program package.[75] An optimization of the geometry for the neutral species was performed in acetonitrile using the integral equation formalism variant of the polarizable continuum model (PCM),[76] and the minimal energy conformation was verified by a frequency calculation. Figure 9 presents the frontier orbital plots of the lowest unoccupied molecular orbital (LUMO) of the studied molecules. As can be observed, the LUMO is almost uniformly distributed along the molecule, with very limited effect from electron-donating or -withdrawing substituents.

Next, we sought to understand the response of the atomic nuclei due to the perturbation of the electron density upon reduction of the diazonium derivatives. To do so, a conceptual density functional theory (CDFT) reactivity descriptor, i.e., the nuclear Fukui function,[77–79] was used. This function allows us to characterize the changes in the force and in positions that the different nuclei experience upon reduction by one electron. The nuclear Fukui function calculations were performed in a finite difference method,[77] which means that two separate calculations, performed on the neutral and reduced species, were carried out using the optimized geometry of the neutral species. These calculations were performed at the DFT/B3LYP[80–82]/6-311G(d,p) level of theory with the Northwest Computational Chemistry Package program package (NWChem 6.8)[83] and enabled us to estimate the magnitude of the change in force (projected vectors) acting on the different nuclei. The magnitudes of the CDFT reactivity descriptor that the atoms of aryl diazonium derivatives experience following the electron attachment are shown in Figure 9.

The nuclear forces indicate that, upon one-electron reduction, the $C–N_2^+$ exhibits the most drastic elongation. This is in line with the reported fragmentation process that occurs along the $C–N_2^+$ bond axis, freeing N_2 and the corresponding aryl radical. It is interesting to note that the magnitude of the force on the nitrogen atom is between 5.18 and 6.88 eV/Å. This magnitude seems to be greater for diazonium with more positive Hammett parameters. These values are also much larger than those recently calculated on halogenated substrate, which showed forces between 2.5 and 4.9 eV/Å for homolytic C–Cl or C–Br bond cleavage, respectively. Hence, these strong forces observed with the diazonium series are in line with very favorable bond dissociation upon reduction.

Please cite this article in press as: Ripak et al., Photosensitized activation of diazonium derivatives for C–B bond formation, Chem Catalysis (2022), https://doi.org/10.1016/j.checat.2022.100490

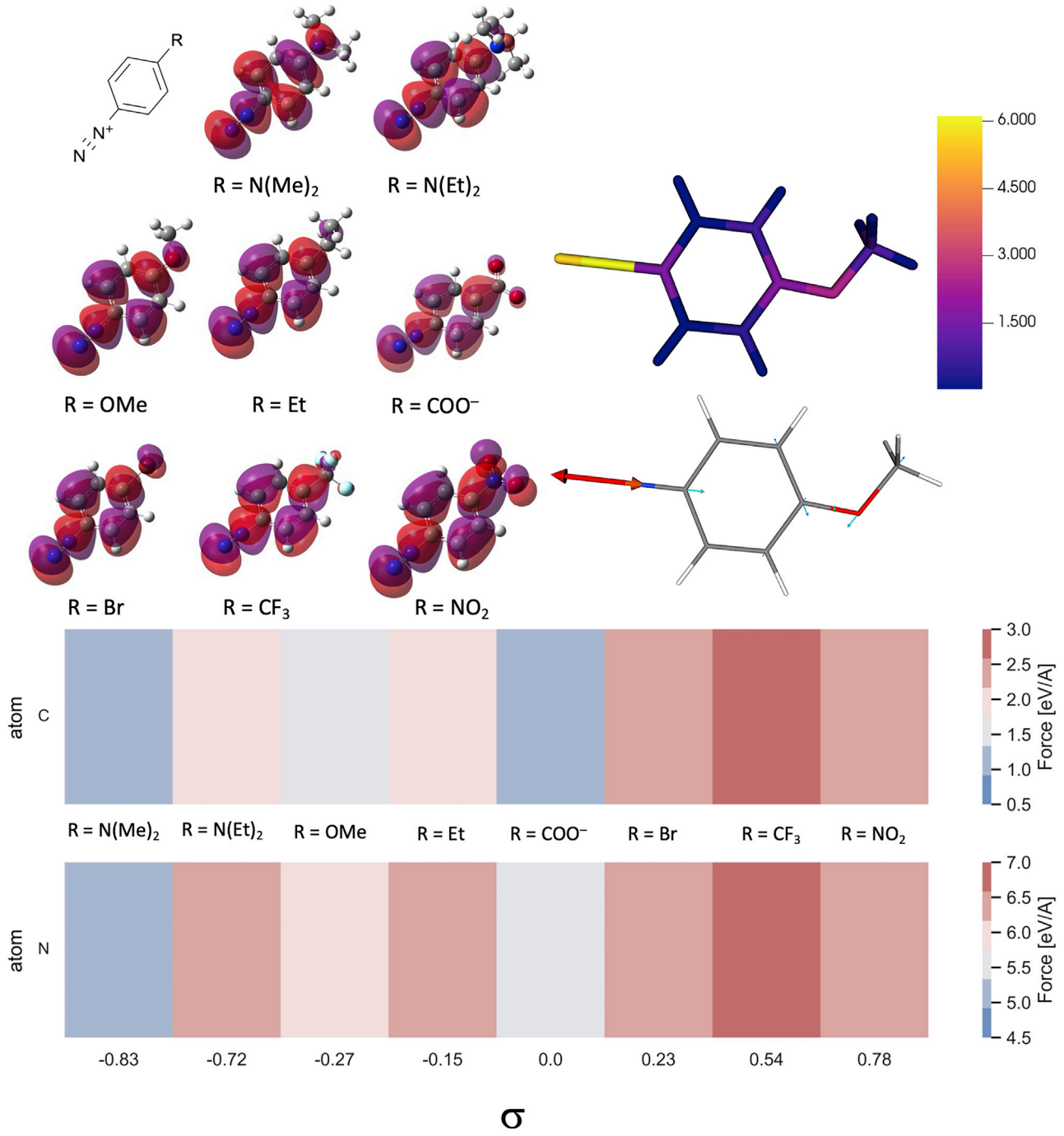

Figure 9. General structure of the aryl diazonium salt and the corresponding LUMO calculated at the MP2 level using the 6-311G(d, p) basis

Force (in eV/Å) on the indicated atom for selected aryl diazonium derivatives, classified according to their Hammett parameters (σ). The color map represents the force experienced by the indicated diazonium upon one-electron reduction.

Photoredox catalysis

With a relatively clear mechanistic picture of excited-state reactivity and charge separation following excited-state electron transfer, we sought to transpose these observations to actual photoredox catalysis. As described in the section

Please cite this article in press as: Ripak et al., Photosensitized activation of diazonium derivatives for C–B bond formation, Chem Catalysis (2022), https://doi.org/10.1016/j.checat.2022.100490

"introduction," there are numerous examples in the literature that use diazonium as starting building block for organic transformation. We decided to use the series of PSs for the visible-light-induced borylation or aryldiazonium salts. This approach was reported by Yan et al. using Eosin Y in acetonitrile at room temperature using 25 W visible-light lamps.[17] This transformation therefore seems compatible with our choice of solvent and with the excited-state lifetime of the different PSs. We focused our endeavor on 4-MeO-benzene diazonium tetrafluoroborate and bis(pinacolato)diboron (B_2pin_2) as borylating agent. For that reaction, 0.5 mmol of diazonium, 0.5 mol % of PS, and 2 equiv of B_2pin_2 were used. The solutions were irradiated using commercial blue, green, or orange light-emitting diodes (LEDs), depending on the absorption profile of the PS (Figure 2). The power was measured and set at 30 mW/cm^2 by adjusting the distance of the LED lamp relative to the reaction round-bottom flask. The spectral profiles of the LEDs are shown in Figure S80. Irradiation for 17 h led to borylation yields of 4-MeO-benzene diazonium tetrafluoroborate that ranged from 9% to 74%, depending on the PS (Figure 10). The yields were determined by ^{1}H NMR using 3,4,5-MeO-benzaldehyde as internal reference. The overall yields are to some extent not essential, but the trend observed between the PSs in otherwise identical conditions is probably the best indicator of reaction success. The lowest yields were observed for the earth-abundant PSs. This is not surprising as both copper PSs showed lack of stability under irradiation or during the course of Stern-Volmer titrations in the presence of diazonium derivatives. The two Fe(III) PSs also led to small yields. As both compounds are very photostable, it seems like the smaller yields are most probably related to the slow kinetics for excited-state electron transfer or to inefficient regeneration of the Fe(III) after oxidation. Indeed, both complexes required much longer irradiation time during photolysis experiments than the other rare earth transition metal PSs (*vide supra*). Yields of 22% with low conversions are obtained with $[Os(bpy)_3]^{2+}$, whereas higher conversions and yields (between 54% and 74%) are obtained with $[Ru(bpy)_3]^{2+}$ and the three iridium(III) PSs. Note that for $[Os(bpy)_3]^{2+}$ a red side product was obtained after reaction, with no presence of PS left. At this stage we are unable to provide clear-cut explanation as to why those yields differ. Indeed, with the exception of $[Ir((dFCF_3)ppy)_2(dtb)]^+$, the ground-state oxidation potential for most of the PSs and quenching rate constant are all in the same range. The difference in yields could come from changes in cage-escape yields or from the relative stability of the different PSs, as 2,2′-bipyridine derivatives could undergo side-reactions with the aryl radicals, but further experiments are needed to elucidate these aspects and remediate the overall moderate yields.

Conclusions

In conclusion, we have investigated the excited-state reactivity of nine PSs with 13 aryl diazonium derivatives. The quenching rate constant were determined and ranged from (1.08–25.1) × 10^9 M^{-1}s^{-1}. Nanosecond transient absorption and steady-state photolysis experiments confirmed that the excited-state quenching proceeded via oxidative electron transfer, efficiently transferring one electron from the excited state to the diazonium. Reaction kinetics recorded in the dark using Fe(III) PSs not only allowed us to obtain kinetic rate constants for electron transfer in the dark but also yielded precious information related to possible discrepancies between electrochemical potential of sacrificial electron donor/acceptors, and potentials determined by kinetic measurements. In addition, these kinetic measurements also informed that the electron transfer process to the diazonium moiety is reversible and that the C–$N_2^{\bullet}$ dissociation occurs on a timescale of 10 ns or shorter. This reversibility was also evident when cage-escape yields were lower than 100%, despite having favorable driving force for electron transfer. Nevertheless, aryl

Please cite this article in press as: Ripak et al., Photosensitized activation of diazonium derivatives for C–B bond formation, Chem Catalysis (2022), https://doi.org/10.1016/j.checat.2022.100490

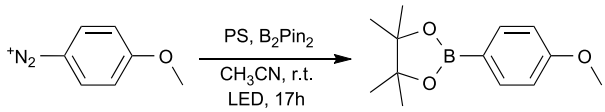

Photosensitizer	Illumination	Conversion	Yield
$[Ru(bpy)_3]^{2+}$	470 nm	100%	63%
$[Os(bpy)_3]^{2+}$	590 nm	27%	22%
$[Ir(ppy)_3]$	470 nm	68%	54%
$[Ir(ppy)_2(dtb)]^+$	470 nm	89%	65%
$[Ir((dFCF_3)ppy)_2(dtb)]^+$	470 nm	100%	74%
$[Fe(phtmeimb)_2]^+$	525 nm	19%	15%
$[Fe(Br\text{-}phtmeimb)_2]^+$	525 nm	23%	11%
$[Cu(bcp)_2]^+$	525 nm	45%	19%
$[Cu(bcp)(DPEPhos)]^+$	470 nm	17%	9%

Reaction conditions: PS (0.5 mol%), MeO-benzene diazonium (0.5 mmol)
B_2pin_2 (1 mmol), CH_3CN (3 mL), 17h, LED 30 mW/cm^2

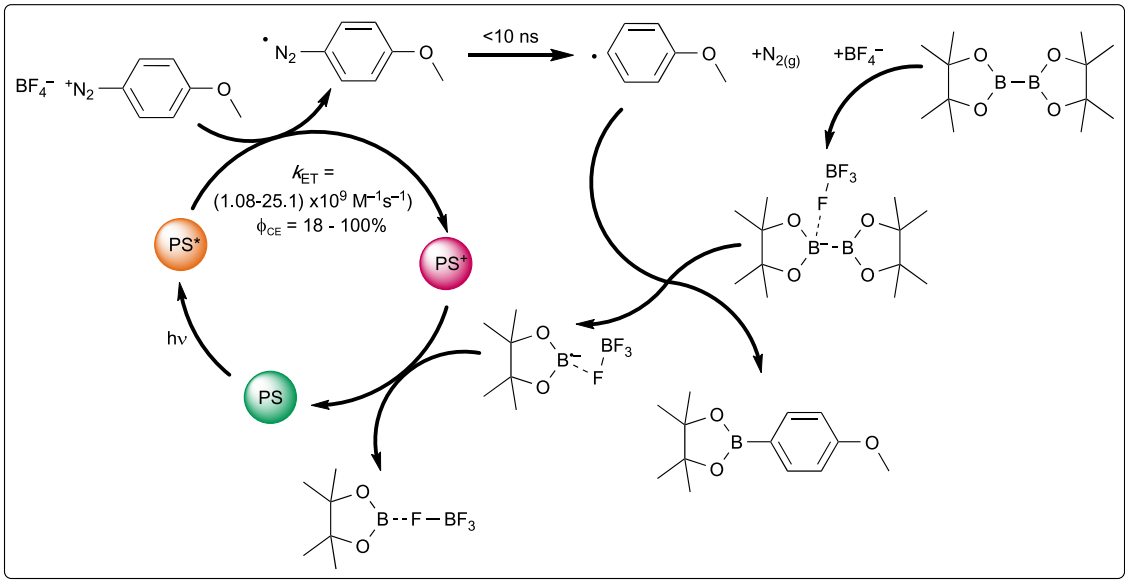

Figure 10. Photoredox catalysis results

Reaction conditions and ^{1}H NMR yields for the indicated reaction using the series of earth-abundant and rare earth transition metal PS (top). Proposed mechanism for the visible-light-mediated borylation of 4-MeO-benzene diazonium (bottom).

diazonium derivatives were shown to lead to very large cage-escape yields that are not often observed in the literature. Indeed, except for some triphenylamine derivatives,[84] most of the cage-escape yields reported thus far for transition metal complexes are in the 10%–40% range. Hence, highly reactive diazonium salts seem to offer new alternatives for more efficient visible-light-mediated transformations. At this stage, we are unable to explain the difference observed in cage-escape yields observed with a series of PSs using the same aryl diazonium. Future studies will focus on further expanding the effect of charge, electrostatic interactions, or dipole moment changes upon electron transfer on these cage-escape yields using inorganic

Please cite this article in press as: Ripak et al., Photosensitized activation of diazonium derivatives for C–B bond formation, Chem Catalysis (2022), https://doi.org/10.1016/j.checat.2022.100490

and organic PSs. Such studies would help determine key parameters that control cage-escape yields and could lead to more efficient light-activated organic transformations with other substrates.

EXPERIMENTAL PROCEDURES

Resource availability

Lead contact

Further information and requests for resources should be directed to and will be fulfilled by the lead contact, Ludovic Troian-Gautier (Ludovic.Troian@uclouvain.be).

Materials availability

All other data supporting the findings of this study are available within the article and the supplemental information or from the lead contact upon reasonable request.

Data and code availability

This study did not generate any datasets.

Materials

Acetonitrile 99.9% (VWR), dry acetonitrile 99.8% (Sigma-Aldrich), dichloromethane 99% (VWR), diethyl ether 99% (VWR), dry diethyl ether 99.5% (Acros Organics), toluene 99.9% (VWR), tetrahydrofuran anhydrous (stabilized with BHT) > 99.5% (TCI), methanol 99.9% (VWR), n-butyllithium solution (1.6 M in hexanes) (Acros Organics), hexamethyldisilazane 98% (Acros Organics), ultra-dry Fe(II) bromide 99.995% (Alfa Aesar), 1-methylimidazole 99% (BASF), NaOH pellet for analysis (VWR), NH_4PF_6 99% (Fluorochem), trimethylsilyl chloride 98% (Acros Organics), dichlorophenylborane 97% (Acros Organics), (4-bromophenyl)trimethylsilane 97% (Ambeed), boron tribromide (1 M in dichloromethane) (Thermo Fisher), nitrosonium tetrafluoroborate 97% (Acors Organics), methoxybenzenediazonium tetrafluoroborate 98% (Thermo Fisher), bromobenzenediazonium tetrafluoroborate 96% (Alfa Aesar), nitrobenzenediazonium tetrafluoroborate 97% (Alfa Aesar), N,N-dimethyl-*p*-phenylenediamine 97% (Acros Organics), N,N-diethyl-*p*-phenylenediamine 97% (Acros Organics), 4-ethylaniline 99.48% (Ambeed), 4-(trifluoromethyl)aniline 99.88% (Ambeed), 4-cyclohexylaniline 97% (Ambeed), ethyl 4-aminobenzoate 99.9% (Ambeed), sodium 4-aminobenzoate 95% (Ambeed), bi(pinacolato)diboron (Fluorochem), tetrabutylammonium tetrafluoroborate 98% (Acros Organics), 3,4,5-trimethoxybenzaldehyde 99% (Acros Organics), SiO_2 40–63 μm (Rocc), and neutral aluminum oxide Brockmann 50–200 μm 60 Å (Acros Organics) were purchased from commercial suppliers and used as received.

Experimental protocols

Synthesis of tris(3-methylimidazolium-1-yl)(4-Br-phenyl)borate bis(hexafluorophosphate)

A solution of 1 M BBr_3 in CH_2Cl_2 (4.8 mL, 4.8 mmol) was placed under argon and cooled to −78°C in a flame-dried round-bottom flask. (4-Bromophenyl)-trimethylsilane (920 mg, 4 mmol) was added in 15 min to the cooled solution and the solution was stirred at −78°C for 1 h and then at room temperature for 3 h. The volatiles were evaporated at 30°C under reduced pressure. The resulting 4-bromodibromophenylborane was used without further purification. It was first dissolved in 10 mL of toluene and this was followed by the dropwise addition of 1-Me-imidazole (1.12 mL, 14 mmol). The solution was stirred for 15 min and TMSCl (1.27 mL, 10 mmol) was then added in one portion. The reaction was then heated for 24 h at 80°C under argon. After reaction, the mixture was evaporated, and the residue was dissolved in water. A saturated solution of ammonium

Please cite this article in press as: Ripak et al., Photosensitized activation of diazonium derivatives for C–B bond formation, Chem Catalysis (2022), https://doi.org/10.1016/j.checat.2022.100490

hexafluorophosphate was then added, which induced precipitation of a beige solid that was collected by filtration, washed with water, and dried under static vacuum. The desired product was then isolated in 80% yield after column chromatography on silica using CH_3CN/MeOH mixtures.

^1H NMR (300 MHz, CD_3CN) δ_H (ppm) 8.00 (s, 3H), 7.60 (d, J = 8.3 Hz, 2H), 7.44 (t, J = 1.7 Hz, 3H), 7.24–6.94 (m, 5H), 3.82 (s, 9H). ^{13}C NMR (75 MHz, CD_3CN) δ_C (ppm) 140.21, 136.42, 135.96, 132.59, 131.50, 125.76, 124.85, 36.54. HRMS (ESI) *m/z*: $[M]^{2+}$ calculated for $C_{18}H_{22}BBrN_6$: 206.05857; found: 206.05891.

Synthesis of Bis(tris(3-methlimidazol-1-ylidene)(phenyl)borate) Fe(III) hexafluorophosphate [Fe(Br-phtmeimb)$_2$]$^+$

A flame-dried and argon-purged 25-mL Schlenk flask, equipped with a stirring bar, was charged with dry HMDS (0.73 mL, 0.565 g, 3.5 mmol) and cooled to 0°C. A solution of n-BuLi (1.6 M in hexanes, 2.25 mL, 3.5 mmol) was added dropwise at 0°C. The reaction mixture was then allowed to reach room temperature and stirred for an additional 30 min. Afterward, the volatiles were slowly removed under reduced pressure to afford a white solid. The resulting product was then solubilized in 3.5 mL of dry THF, forming the corresponding LiHMDS solution.

A flame-dried and argon-purged 50-mL Schlenk flask equipped with a stirring bar was charged with tris(3-methylimidazolium-1-yl)(4-Br-phenyl)borate bis(hexafluorophosphate) (0.703 g, 1.0 mmol) and the solid was dried under vacuum for 2 h before being purged under argon. Dry THF (20 mL) was then added under argon. The mixture was cooled to −78°C and the previously obtained LiHMDS solution was added dropwise. The reaction mixture was stirred at this temperature for 30 min. A solution of anhydrous $FeBr_2$ was prepared by adding $FeBr_2$ (0.108 g, 0.5 mmol) into a flame-dried and argon-purged 10-mL Schlenk flask followed by 10 mL of dry THF. The mixture was sonicated for 20 min to ensure solubilization of the iron source. Afterward, the cooling bath was removed and the solution of $FeBr_2$ was added dropwise to the deprotonated ligand solution. The reaction mixture was allowed to slowly reach room temperature under argon and then was stirred at room temperature for 72 h in the dark. Upon exposure to air, the solution became dark red and the solvent was removed under reduced pressure. The resulting residue was dissolved in 30 mL of CH_2Cl_2, filtered through a porosity 4 frit, washed with 2 × 15 mL of CH_2Cl_2, and the filtrate was evaporated under reduced pressure, resulting in a dark red solid. The residue was then solubilized in a minimum amount of CH_3CN and poured in approximately 200 mL of diethyl ether, which induced precipitation of a red solid that was collected by filtration and washed with 3 × 30 mL of diethyl ether and dried under vacuum. The resulting solid was then washed with methanol, filtered, and the precipitate was washed with methanol before being dried under static vacuum. The desired compound was obtained as a red powder (153 mg, 30%).

^1H NMR (300 MHz, CD_3CN) δ_H (ppm) 14.77 (d, J = 7.3 Hz, 4H), 10.60 (d, J = 5.8 Hz, 4H), 4.97 (s, 18H), 1.37 (s, 6H), −12.46 (s, 6H). HRMS (ESI) *m/z*: $[M]^+$ calculated for $C_{36}H_{38}B_2Br_2N_{12}Fe$: 876.12278; found: 876.12226.

General procedure for the synthesis of aryl diazonium derivatives

Aniline (0.71 mmol) was dissolved on 3 mL of argon-purged acetonitrile. The solution was kept under argon and cooled to −40°C. $NOBF_4$ (261 mg, 1.77 mmol) was added in one portion and the medium was allowed to stir at −40°C for 2 h. After reaction, the mixture was evaporated under reduced pressure and the residue was triturated three times with 10 mL of diethyl ether. The formed precipitate was isolated and dried under

Please cite this article in press as: Ripak et al., Photosensitized activation of diazonium derivatives for C–B bond formation, Chem Catalysis (2022), https://doi.org/10.1016/j.checat.2022.100490

reduced pressure, which afforded the corresponding diazonium with >95% yields. The diazonium derivatives were then stored in the freezer at −18°C.

Note that, although we have not encountered any problem, diazonium salts are potentially explosive and should be handled with appropriate precautions. The use of tetrafluoroborate counter-ions increases the stability of the resulting diazonium salts. Calix[4]arene derivatives have been shown to exhibit thermal stability up to 150°C.

4-Trifluoromethyl-benzene diazonium tetrafluoroborate. ^{1}H NMR (CD_3CN, 300 MHz) δ_H (ppm) 8.69 (d, J = 8.7 Hz, 2H), 8.23 (d, J = 8.8 Hz, 2H).

4-Cyclohexyl)benzene diazonium tetrafluoroborate. ^{1}H NMR (CD_3CN, 300 MHz) δ_H (ppm) 8.38 (d, J = 8.5 Hz, 2H), 7.78 (d, J = 8.5 Hz, 2H), 2.83 (m, 1H), 1.92–1.67 (m, 5H), 1.57–1.21 (m, 5H).

4-Ethyl-benzene diazonium tetrafluoroborate. ^{1}H NMR ($CDCl_3$, 300 MHz) δ_H (ppm) 8.51 (d, J = 8.4 Hz, 2H), 7.62 (d, J = 8.3 Hz, 2H), 2.85 (q J = 7.6 Hz, 2H), 1.28 (t, J = 7.5 Hz, 3H).

4-Carboxylate-benzene diazonium. ^{1}H NMR (D_2O, 300 MHz) δ_H (ppm) 8.65 (dt, J = 9.1, 2.0 Hz, 2H), 8.37 (dt, J = 8.9, 2.0 Hz, 2H).

4-Ethylester-benzene diazonium tetrafluoroborate. ^{1}H NMR (CD_3CN, 300 MHz) δ_H (ppm) 8.58 (dt, J = 9.1, 1.9 Hz, 2H), 8.42 (dt, J = 9.1, 2.0 Hz, 2H), 4.44 (q, J = 7.1 Hz, 2H), 1.39 (t, J = 7.1 Hz, 2H).

4-N,N-dimethylamino-benzene diazonium tetrafluoroborate. ^{1}H NMR (CD_3CN, 300 MHz) δ_H (ppm) 7.98 (d, J = 9.8 Hz, 2H), 6.93 (d, J = 9.8 Hz, 2H), 3.26 (s, 6H).

4-N,N-diethylamino-benzene diazonium tetrafluoroborate. ^{1}H NMR (CD_3CN, 300 MHz) δ_H (ppm) 7.97 (d, J = 9.8 Hz, 2H), 6.94 (d, J = 9.8 Hz, 2H), 3.61 (q, J = 7.2 Hz, 4H), 1.23 (t, J = 7.2 Hz, 6H).

General procedure for the photoredox catalysis experiments

4-MeO-benzene diazonium tetrafluoroborate (111 mg, 0.5 mmol), bis(pinacolato)diboron (254 mg, 1 mmol), and the PS (0.5 mol %) were placed in 3 mL of argon-purged acetonitrile. The solution was kept under argon and was irradiated with the appropriate LED for 17 h. After reaction, the mixture was evaporated to dryness and the residue was dried under static vacuum for 24 h before being subjected to quantitative NMR using 3,4,5-trimethoxy benzaldehyde as internal reference. The final products can also be purified on silica gel using cyclohexane/ethyl acetate mixtures as eluent.

UV-vis spectroscopy

UV-vis absorption spectra were recorded on a Shimadzu UV-1700 with a 1-cm path length quartz cell.

Time-resolved PL

Time-resolved PL spectra were recorded on an LP980-K spectrometer from Edinburgh Instruments (see "transient absorption spectroscopy" for full description). The optically diluted samples were excited with pulsed light and the excited-state lifetime was measured on a PMT LP detector (Hamamatsu R928), which covers the

Please cite this article in press as: Ripak et al., Photosensitized activation of diazonium derivatives for C–B bond formation, Chem Catalysis (2022), https://doi.org/10.1016/j.checat.2022.100490

spectral range from 185 to 870 nm. An average of 30 scans per measurement was used.

Electrochemistry

Cyclic voltammetry was performed with an Autolab PGSTAT 100 potentiostat using a standard three-electrode-cell; i.e., a glassy carbon disk working electrode (approximate area = 0.03 cm^2), a platinum wire counter electrode, and an aqueous Ag/AgCl reference electrode (salt bridge: 3 M KCl/saturated AgCl). Experiments were performed in dry 0.1 M tetrabutylammonium perchlorate acetonitrile electrolyte, and the samples were purged with argon before each measurement. For comparison purposes, the electrochemical potentials were converted to NHE by adding 0.197 V.

Steady-state PL

Room-temperature steady-state PL spectra were recorded on a Horiba Scientific-FL-1000 fluorimeter and were corrected by calibration of the instrument's response with a standard tungsten-halogen lamp. The PL intensity was integrated for 0.1 s at 1-nm resolution and averaged over three scans. Alternatively, some steady-state PL spectra were recorded on a Varian Cary Eclipse spectrometer and were not corrected for the instrument's response.

Stern-Volmer experiments

A PS stock solution with an absorbance of ~0.1–~0.2 at the excitation wavelength was prepared in acetonitrile containing 0.1 M $TBABF_4$. The stock solution was purged with argon for 30 min. Aryl diazonium tetrafluoroborate salts were then weighted in scintillation vials to reach a final desired concentration between 20 and 30 mM. Then 2 mL of the PS stock solution were added to the scintillation vial kept under argon, and 3 mL of the stock solution were transferred to a quartz cuvette equipped with a 24/40 joint, also kept under argon. The cuvette and the scintillation vials were purged with argon for another 5 min. The desired aryl diazonium tetrafluoroborate quencher was then gradually added to the cuvette. This allowed us to increase the concentration of quencher while keeping the concentration of PS constant. The excited-state quenching was monitored by time-resolved spectroscopy using the LP980-K spectrometer from Edinburgh Instruments (see below) or by steady-state PL when $[Fe(phtmeimb)_2]^+$ or $[Fe(Br\text{-}phtmeimb)_2]^+$ were used. The decrease of excited-state lifetime or PL is directly related to the concentration of quencher and the respective Stern-Volmer plots were extrapolated using Equation 5. The quenching rate constant (k_q) was then determined by dividing the slope by the initial lifetime without any quencher, determined for each experiment.

$$\frac{\sum(PLI_0)}{\sum(PLI)} = \frac{\tau_0}{\tau} = 1 + K_{SV}[Q] = 1 + k_q\tau_0[Q] \qquad \text{(Equation 5)}$$

Transient absorption spectroscopy

Nanosecond transient absorption measurements were recorded on an LP980-K spectrometer from Edinburgh Instruments equipped with an iCCD detector from Andor (DH320T). The excitation source was a tunable Nd:YAG Laser NT342 Series from EKSPLA. The third harmonic (355 nm) at 150 mJ was directed into an optical parametric oscillator (OPO) to enable wavelength tuning starting from 410 nm. The laser power was then attenuated to reach appreciable signal/noise and the integrity of the samples was verified by UV-vis measurements. The LP980-K is equipped with a symmetrical Czerny-Turner monochromator. For single-wavelength absorption changes, a 1,800 g mm^{-1} grating, blazed at 500 nm is used, which affords wavelength coverage from 200 to 900 nm. For spectral mode (iCCD), a 150 g mm^{-1} grating, blazed at 500 nm is used, offering a wavelength coverage of 540 nm over

Please cite this article in press as: Ripak et al., Photosensitized activation of diazonium derivatives for C–B bond formation, Chem Catalysis (2022), https://doi.org/10.1016/j.checat.2022.100490

the full wavelength range extending from 250 to 900 nm. Single-wavelength absorption changes were monitored using a PMT LP detector (Hamamatsu R928), which covers the spectral range from 185 to 870 nm. The probe was a 150 W ozone-free xenon short arc lamp (OSRAM XBO 150W/CR OFR) that was pulsed at the same frequency of the laser. The excitation wavelength depended on the PSs but, in all cases, the concentration at the excitation wavelength was adjusted to reach absorbance values between 0.3 and 0.5. All measurements were performed in argon-purged acetonitrile containing 0.1 M $TBABF_4$ at room temperature. An average of 30–90 scans per measurement was used.

Quantum mechanical calculations

MP2 calculations have been performed using the Gaussian16 program,[75] applying default procedures, integration grids, algorithms, and parameters. Selected diazonium salts were considered in this theoretical study. The geometry of the ground-state species was optimized at the MP2/6-311G(d,p) level. MP2 with the same basis set was used to study the effect of electron correlation on the calculated density. Additional calculations were done with the NWChem program package[83] in order to calculate the nuclear Fukui function.[78,79] The nuclear Fukui function characterizes the changes in the forces (energy gradient) that nuclei experience when the total number of electrons of the system is changed and can be calculated using the finite difference method.[77] For that, two separate B3LYP/6-311G(d,p) calculations, performed on the ground and reduced species, are carried out, both with the geometry of the ground state. The magnitude of the change in force acting on the nuclei was estimated as well as the projected forces along the bonds involving the nuclei. These were depicted as vectors with the origin located on the nuclei. Both quantities were visualized using VisIt 3.1.4[85] and can help to interpret some trends in nuclear reactivity as they pertain to the initial mechanistic steps of electron-induced attachment.[86]

SUPPLEMENTAL INFORMATION

Supplemental information can be found online at https://doi.org/10.1016/j.checat.2022.100490.

ACKNOWLEDGMENTS

Financial support was provided to A.R. by the F.R.S.-FNRS (FRIA fellowship). This work was supported by the Fonds de la Recherche Scientifique (F.R.S.-FNRS) under grant no. U.N021.21 (B.E.). L.T.-G. is a Chercheur Qualifié of the Fonds de la Recherche Scientifique-FNRS. S.D.K., B.E., and L.T.-G. gratefully acknowledge the UCLouvain for financial support. Computational resources have been provided by the Consortium des Équipements de Calcul Intensif (CÉCI), funded by the Fonds de la Recherche Scientifique de Belgique (F.R.S.-FNRS) under grant no. 2.5020.11 and by the Walloon Region. Financial support was provided to U.K.T. by W.W. Caruth, Jr. Endowed Scholarship, Welch Foundation (I-1748), National Institutes of Health (R01GM102604), American Chemical Society Petroleum Research Fund (59177-ND1), and Teva Pharmaceuticals Marc A. Goshko Memorial Grant (60011-TEV). Financial support was provided to C.A.V. by Sarah and Frank McKnight Fund Graduate Fellowship.

AUTHOR CONTRIBUTIONS

A.R. and S.D.K. conducted the experiments. C.A.V. performed initial photoreactions using $[Ru(bpy)_3]^{2+}$ and MeO-benzene diazonium. E.C. designed and performed computational experiments. R.N.S. performed the kinetic modeling for

the dark state reactivity. I.J. provided the calix[4]arene derivatives. L.T.-G., B.E., and U.K.T. conceptualized, designed the experiments, and supervised the research. All the authors analyzed and interpreted the data and wrote and edited the manuscript.

DECLARATION OF INTERESTS

The authors declare no competing interests.

INCLUSION AND DIVERSITY

We support inclusive, diverse, and equitable conduct of research.

Received: September 7, 2022
Revised: November 3, 2022
Accepted: December 8, 2022
Published: January 4, 2023

REFERENCES

1. Griess, J.P., and Hofmann, A.W.V. (1864). XVIII. On a new series of bodies in which nitrogen is substituted for hydrogen. Phil. Trans. Roy. Soc. Lond. *154*, 667–731. https://doi.org/10.1098/rstl.1864.0018.

2. Mo, F., Qiu, D., Zhang, L., and Wang, J. (2021). Recent development of aryl diazonium chemistry for the derivatization of aromatic compounds. Chem. Rev. *121*, 5741–5829. https://doi.org/10.1021/acs.chemrev.0c01030.

3. Mo, F., Dong, G., Zhang, Y., and Wang, J. (2013). Recent applications of arene diazonium salts in organic synthesis. Org. Biomol. Chem. *11*, 1582–1593. https://doi.org/10.1039/C3OB27366K.

4. Troian-Gautier, L., Mattiuzzi, A., Reinaud, O., Lagrost, C., and Jabin, I. (2020). Use of calixarenes bearing diazonium groups for the development of robust monolayers with unique tailored properties. Org. Biomol. Chem. *18*, 3624–3637. https://doi.org/10.1039/D0OB00070A.

5. Hari, D.P., and König, B. (2013). The photocatalyzed Meerwein arylation: classic reaction of aryl diazonium salts in a new light. Angew. Chem. Int. Ed. Engl. *52*, 4734–4743. https://doi.org/10.1002/anie.201210276.

6. Bélanger, D., and Pinson, J. (2011). Electrografting: a powerful method for surface modification. Chem. Soc. Rev. *40*, 3995–4048. https://doi.org/10.1039/C0CS00149J.

7. Babu, S.S., Muthuraja, P., Yadav, P., and Gopinath, P. (2021). Aryldiazonium salts in photoredox catalysis – recent trends. Adv. Synth. Catal. *363*, 1782–1809. https://doi.org/10.1002/adsc.202100136.

8. Delamar, M., Hitmi, R., Pinson, J., and Saveant, J.M. (1992). Covalent modification of carbon surfaces by grafting of functionalized aryl radicals produced from electrochemical reduction of diazonium salts. J. Am. Chem. Soc. *114*, 5883–5884. https://doi.org/10.1021/ja00040a074.

9. Pinson, J., and Podvorica, F. (2005). Attachment of organic layers to conductive or semiconductive surfaces by reduction of diazonium salts. Chem. Soc. Rev. *34*, 429–439. https://doi.org/10.1039/B406228K.

10. Troian-Gautier, L., Valkenier, H., Mattiuzzi, A., Jabin, I., den Brande, N.V., Mele, B.V., Hubert, J., Reniers, F., Bruylants, G., Lagrost, C., and Leroux, Y. (2016). Extremely robust and post-functionalizable gold nanoparticles coated with calix[4]arenes via metal-carbon bonds. Chem. Commun. *52*, 10493–10496. https://doi.org/10.1039/C6CC04534K.

11. Mattiuzzi, A., Jabin, I., Mangeney, C., Roux, C., Reinaud, O., Santos, L., Bergamini, J.-F., Hapiot, P., and Lagrost, C. (2012). Electrografting of calix[4]arenediazonium salts to form versatile robust platforms for spatially controlled surface functionalization. Nat. Commun. *3*, 1130. https://doi.org/10.1038/ncomms2121.

12. Cano-Yelo, H., and Deronzier, A. (1984). Photo-oxidation of tris(2, 2′-bipyridine)ruthenium(II) by para-substituted benzene diazonium salts in acetonitrile. Two-compartment photoelectrochemical cell applications. J. Chem. Soc., Faraday Trans. *80*, 3011–3019. https://doi.org/10.1039/F19848003011.

13. Cano-Yelo, H., and Deronzier, A. (1984). Photo-oxidation of some carbinols by the Ru(II) polypyridyl complex-aryl diazonium salt system. Tetrahedron Lett. *25*, 5517–5520. https://doi.org/10.1016/S0040-4039(01)81614-2.

14. Hari, D.P., Schroll, P., and König, B. (2012). Metal-free, visible-light-mediated direct C–H arylation of heteroarenes with aryl diazonium salts. J. Am. Chem. Soc. *134*, 2958–2961. https://doi.org/10.1021/ja212099r.

15. Louvel, D., Chelagha, A., Rouillon, J., Payard, P.-A., Khrouz, L., Monnereau, C., and Tlili, A. (2021). Metal-free visible-light synthesis of arylsulfonyl fluorides: scope and mechanism. Chemistry *27*, 8704–8708. https://doi.org/10.1002/chem.202101056.

16. Kalyani, D., McMurtrey, K.B., Neufeldt, S.R., and Sanford, M.S. (2011). Room-temperature C–H arylation: merger of Pd-catalyzed C–H functionalization and visible-light photocatalysis. J. Am. Chem. Soc. *133*, 18566–18569. https://doi.org/10.1021/ja208068w.

17. Yu, J., Zhang, L., and Yan, G. (2012). Metal-free, visible light-induced borylation of aryldiazonium salts: a simple and green synthetic route to arylboronates. Adv. Synth. Catal. *354*, 2625–2628. https://doi.org/10.1002/adsc.201200416.

18. Lentz, C., Marcélis, L., Troian-Gautier, L., Robeyns, K., Cauët, E., and Elias, B. (2021). Excited-state behavior and photoinduced electron transfer of pH-sensitive Ir(III) complexes with cyclometallation (C/N–) ratios between 0/6 and 3/3. J. Photochem. Photobiol. Chem. *405*, 112957. https://doi.org/10.1016/j.jphotochem.2020.112957.

19. Aydogan, A., Bangle, R.E., Cadranel, A., Turlington, M.D., Conroy, D.T., Cauët, E., Singleton, M.L., Meyer, G.J., Sampaio, R.N., Elias, B., and Troian-Gautier, L. (2021). Accessing photoredox transformations with an iron(III) photosensitizer and green light. J. Am. Chem. Soc. *143*, 15661–15673. https://doi.org/10.1021/jacs.1c06081.

20. Kjær, K.S., Kaul, N., Prakash, O., Chábera, P., Rosemann, N.W., Honarfar, A., Gordivska, O., Fredin, L.A., Bergquist, K.-E., Häggström, L., et al. (2019). Luminescence and reactivity of a charge-transfer excited iron complex with nanosecond lifetime. Science *363*, 249–253. https://doi.org/10.1126/science.aau7160.

21. Prakash, O., Lindh, L., Kaul, N., Rosemann, N.W., Losada, I.B., Johnson, C., Chábera, P., Ilic, A., Schwarz, J., Gupta, A.K., et al. (2022). Photophysical integrity of the iron(III) scorpionate framework in iron(III)–NHC complexes with long-lived 2LMCT excited states. Inorg. Chem. *61*, 17515–17526. https://doi.org/10.1021/acs.inorgchem.2c02410.

22. Kaufmann, D. (1987). Borylierung von Arylsilanen, I Ein allgemeiner, einfacher und selektiver Zugang zu Phenyldihalogenboranen. Chem. Ber. *120*, 853–854. https://doi.org/10.1002/cber.19871200527.

23. Forshaw, A.P., Bontchev, R.P., and Smith, J.M. (2007). Oxidation of the tris(carbene)borate

Please cite this article in press as: Ripak et al., Photosensitized activation of diazonium derivatives for C–B bond formation, Chem Catalysis (2022), https://doi.org/10.1016/j.checat.2022.100490

complex PhB(MeIm)3MnI(CO)3 to MnIV [PhB(MeIm)3]2(OTf)2. Inorg. Chem. *46*, 3792–3794. https://doi.org/10.1021/ic070187w.

24. Troian-Gautier, L., Martínez-Tong, D.E., Hubert, J., Reniers, F., Sferrazza, M., Mattiuzzi, A., Lagrost, C., and Jabin, I. (2016). Controlled modification of polymer surfaces through grafting of calix[4]arene-tetradiazoate salts. J. Phys. Chem. C *120*, 22936–22945. https://doi.org/10.1021/acs.jpcc.6b06143.

25. Hansch, C., Leo, A., and Taft, R.W. (1991). A survey of Hammett substituent constants and resonance and field parameters. Chem. Rev. *91*, 165–195. https://doi.org/10.1021/cr00002a004.

26. Sachdeva, G., Vaya, D., Srivastava, C.M., Kumar, A., Rawat, V., Singh, M., Verma, M., Rawat, P., and Rao, G.K. (2022). Calix[n]arenes and its derivatives as organocatalysts. Coord. Chem. Rev. *472*, 214791. https://doi.org/10.1016/j.ccr.2022.214791.

27. Kober, E.M., and Meyer, T.J. (1982). Concerning the absorption spectra of the ions M(bpy)32+ (M = Fe, Ru, Os; bpy = 2, 2′-bipyridine). Inorg. Chem. *21*, 3967–3977. https://doi.org/10.1021/ic00141a021.

28. Cerfontaine, S., Wehlin, S.A.M., Elias, B., and Troian-Gautier, L. (2020). Photostable polynuclear ruthenium(II) photosensitizers competent for dehalogenation photoredox catalysis at 590 nm. J. Am. Chem. Soc. *142*, 5549–5555. https://doi.org/10.1021/jacs.0c01503.

29. Juris, A., Balzani, V., Barigelletti, F., Campagna, S., Belser, P., and von Zelewsky, A. (1988). Ru(II) polypyridine complexes: photophysics, photochemistry, eletrochemistry, and chemiluminescence. Coord. Chem. Rev. *84*, 85–277. https://doi.org/10.1016/0010-8545(88)80032-8.

30. Maurer, A.B., and Meyer, G.J. (2020). Stark spectroscopic evidence that a spin change accompanies light absorption in transition metal polypyridyl complexes. J. Am. Chem. Soc. *142*, 6847–6851. https://doi.org/10.1021/jacs.9b13602.

31. Ruthkosky, M., Castellano, F.N., and Meyer, G.J. (1996). Photodriven electron and energy transfer from copper phenanthroline excited states. Inorg. Chem. *35*, 6406–6412. https://doi.org/10.1021/ic960503z.

32. Luo, S.-P., Mejía, E., Friedrich, A., Pazidis, A., Junge, H., Surkus, A.-E., Jackstell, R., Denurra, S., Gladiali, S., Lochbrunner, S., and Beller, M. (2013). Photocatalytic water reduction with copper-based photosensitizers: a noble-metal-free system. Angew. Chem. Int. Ed. Engl. *52*, 419–423. https://doi.org/10.1002/anie.201205915.

33. Kirchhoff, J.R., Gamache, R.E., Jr., Blaskie, M.W., Del Paggio, A.A., Lengel, R.K., and McMillin, D.R. (1983). Temperature dependence of luminescence from Cu(NN)2+ systems in fluid solution. Evidence for the participation of two excited states. Inorg. Chem. *22*, 2380–2384. https://doi.org/10.1021/ic00159a008.

34. Ichinaga, A.K., Kirchhoff, J.R., McMillin, D.R., Dietrich-Buchecker, C.O., Marnot, P.A., and Sauvage, J.P. (1987). Charge-transfer absorption and emission of Cu(NN)2+ systems. Inorg. Chem. *26*, 4290–4292. https://doi.org/10.1021/ic00272a030.

35. McCusker, C.E., Chakraborty, A., and Castellano, F.N. (2014). Excited state equilibrium induced lifetime extension in a dinuclear platinum(II) complex. J. Phys. Chem. A *118*, 10391–10399. https://doi.org/10.1021/jp503827e.

36. Yarnell, J.E., McCusker, C.E., Leeds, A.J., Breaux, J.M., and Castellano, F.N. (2016). Exposing the excited-state equilibrium in an IrIII bichromophore: a combined time resolved spectroscopy and computational study. Eur. J. Inorg. Chem. *2016*, 1808–1818. https://doi.org/10.1002/ejic.201600194.

37. Ito, A., and Meyer, T.J. (2012). The Golden Rule. Application for fun and profit in electron transfer, energy transfer, and excited-state decay. Phys. Chem. Chem. Phys. *14*, 13731–13745. https://doi.org/10.1039/C2CP41658A.

38. Vlcek, A.A., Dodsworth, E.S., Pietro, W.J., and Lever, A.B.P. (1995). Excited state redox potentials of ruthenium diimine complexes; correlations with ground state redox potentials and ligand parameters. Inorg. Chem. *34*, 1906–1913. https://doi.org/10.1021/ic00111a043.

39. Prier, C.K., Rankic, D.A., and MacMillan, D.W.C. (2013). Visible light photoredox catalysis with transition metal complexes: applications in organic synthesis. Chem. Rev. *113*, 5322–5363. https://doi.org/10.1021/cr300503r.

40. Rosemann, N.W., Chábera, P., Prakash, O., Kaufhold, S., Wärnmark, K., Yartsev, A., and Persson, P. (2020). Tracing the full bimolecular photocycle of iron(III)–Carbene light harvesters in electron-donating solvents. J. Am. Chem. Soc. *142*, 8565–8569. https://doi.org/10.1021/jacs.0c00755.

41. Bürgin, T.H., Glaser, F., and Wenger, O.S. (2022). Shedding light on the oxidizing properties of spin-flip excited states in a CrIII polypyridine complex and their use in photoredox catalysis. J. Am. Chem. Soc. *144*, 14181–14194. https://doi.org/10.1021/jacs.2c04465.

42. Bevernaegie, R., Wehlin, S.A.M., Piechota, E.J., Abraham, M., Philouze, C., Meyer, G.J., Elias, B., and Troian-Gautier, L. (2020). Improved visible light absorption of potent iridium(III) photo-oxidants for excited-state electron transfer chemistry. J. Am. Chem. Soc. *142*, 2732–2737. https://doi.org/10.1021/jacs.9b12108.

43. Rehm, D., and Weller, A. (1970). Kinetics of fluorescence quenching by electron and H-atom transfer. Isr. J. Chem. *8*, 259–271. https://doi.org/10.1002/ijch.197000029.

44. Deetz, A.M., Troian-Gautier, L., Wehlin, S.A.M., Piechota, E.J., and Meyer, G.J. (2021). On the determination of halogen atom reduction potentials with photoredox catalysts. J. Phys. Chem. A *125*, 9355–9367. https://doi.org/10.1021/acs.jpca.1c06772.

45. Miller, J.R., Calcaterra, L.T., and Closs, G.L. (1984). Intramolecular long-distance electron transfer in radical anions. The effects of free energy and solvent on the reaction rates. J. Am. Chem. Soc. *106*, 3047–3049. https://doi.org/10.1021/ja00322a058.

46. Xiao, P., Dumur, F., Zhang, J., Fouassier, J.P., Gigmes, D., and Lalevée, J. (2014). Copper complexes in radical photoinitiating systems: applications to free radical and cationic polymerization upon visible LEDs. Macromolecules *47*, 3837–3844. https://doi.org/10.1021/ma5006793.

47. Kuang, S.-M., Cuttell, D.G., McMillin, D.R., Fanwick, P.E., and Walton, R.A. (2002). Synthesis and structural characterization of Cu(I) and Ni(II) complexes that contain the bis [2-(diphenylphosphino)phenyl]ether ligand. Novel emission properties for the Cu(I) species. Inorg. Chem. *41*, 3313–3322. https://doi.org/10.1021/ic0201809.

48. Scaltrito, D.V., Thompson, D.W., O'Callaghan, J.A., and Meyer, G.J. (2000). MLCT excited states of cuprous bis-phenanthroline coordination compounds. Coord. Chem. Rev. *208*, 243–266. https://doi.org/10.1016/S0010-8545(00)00309-X.

49. Kaeser, A., Mohankumar, M., Mohanraj, J., Monti, F., Holler, M., Cid, J.-J., Moudam, O., Nierengarten, I., Karmazin-Brelot, L., Duhayon, C., et al. (2013). Heteroleptic copper(I) complexes prepared from phenanthroline and bis-phosphine ligands. Inorg. Chem. *52*, 12140–12151. https://doi.org/10.1021/ic4020042.

50. Nishikawa, M., Kakizoe, D., Saito, Y., Ohishi, T., and Tsubomura, T. (2017). Redox properties of copper(I) complex bearing 4, 7-diphenyl-2, 9-dimethyl-1, 10-phenanthroline and 1, 4-Bis(diphenylphosphino)butane ligands and effects of light in the presence of chloroform. Bull. Chem. Soc. Jpn. *90*, 286–288. https://doi.org/10.1246/bcsj.20160339.

51. Zhang, Y., Heberle, M., Wächtler, M., Karnahl, M., and Dietzek, B. (2016). Determination of side products in the photocatalytic generation of hydrogen with copper photosensitizers by resonance Raman spectroelectrochemistry. RSC Adv. *6*, 105801–105805. https://doi.org/10.1039/C6RA21469J.

52. Moonshiram, D., Garrido-Barros, P., Gimbert-Suriñach, C., Picón, A., Liu, C., Zhang, X., Karnahl, M., and Llobet, A. (2018). Elucidating the nature of the excited state of a heteroleptic copper photosensitizer by using time-resolved X-ray absorption spectroscopy. Chemistry *24*, 6464–6472. https://doi.org/10.1002/chem.201800330.

53. Wodon, M., De Kreijger, S., Sampaio, R.N., Elias, B., and Troian-Gautier, L. (2022). Accumulation of mono-reduced [Ir(piq)2(LL)] photosensitizers relevant for solar fuels production. Photochem. Photobiol. Sci. *21*, 1433–1444. https://doi.org/10.1007/s43630-022-00233-z.

54. Shaw, G.B., Grant, C.D., Shirota, H., Castner, E.W., Meyer, G.J., and Chen, L.X. (2007). Ultrafast structural rearrangements in the MLCT excited state for copper(I) bis-phenanthrolines in solution. J. Am. Chem. Soc. *129*, 2147–2160. https://doi.org/10.1021/ja067271f.

55. Fajardo, J., Jr., Barth, A.T., Morales, M., Takase, M.K., Winkler, J.R., and Gray, H.B. (2021). Photoredox catalysis mediated by tungsten(0) arylisocyanides. J. Am. Chem. Soc. *143*, 19389–19398. https://doi.org/10.1021/jacs.1c07617.

Please cite this article in press as: Ripak et al., Photosensitized activation of diazonium derivatives for C–B bond formation, Chem Catalysis (2022), https://doi.org/10.1016/j.checat.2022.100490

56. Glaser, F., Kerzig, C., and Wenger, O.S. (2021). Sensitization-initiated electron transfer via upconversion: mechanism and photocatalytic applications. Chem. Sci. *12*, 9922–9933. https://doi.org/10.1039/D1SC02085D.

57. Ilic, A., Schwarz, J., Johnson, C., de Groot, L.H.M., Kaufhold, S., Lomoth, R., and Wärnmark, K. (2022). Photoredox catalysis via consecutive 2LMCT- and 3MLCT-excitation of an Fe(iii/ii)–N-heterocyclic carbene complex. Chem. Sci. *13*, 9165–9175. https://doi.org/10.1039/D2SC02122F.

58. Aydogan, A., Bangle, R.E., De Kreijger, S., Dickenson, J.C., Singleton, M.L., Cauët, E., Cadranel, A., Meyer, G.J., Elias, B., Sampaio, R.N., and Troian-Gautier, L. (2021). Mechanistic investigation of a visible light mediated dehalogenation/cyclisation reaction using iron(iii), iridium(iii) and ruthenium(ii) photosensitizers. Catal. Sci. Technol. *11*, 8037–8051. https://doi.org/10.1039/D1CY01771C.

59. Olmsted, J., and Meyer, T.J. (1987). Factors affecting cage escape yields following electron-transfer quenching. J. Phys. Chem. A *91*, 1649–1655. https://doi.org/10.1021/j100290a071.

60. Kalyanasundaram, K., and Neumann-Spallart, M. (1982). Influence of added salts on the cage escape yields in the photoredox quenching of Ru(bpy)2+3 excited states. Chem. Phys. Lett. *88*, 7–12. https://doi.org/10.1016/0009-2614(82)80059-6.

61. Mallouk, T.E., Krueger, J.S., Mayer, J.E., and Dymond, C.M.G. (1989). Reductive quenching of ruthenium polypyridyl sensitizers by cyanometalate complexes. Inorg. Chem. *28*, 3507–3510. https://doi.org/10.1021/ic00317a023.

62. Yoshimura, A., Hoffman, M.Z., and Sun, H. (1993). An evaluation of the excited state absorption spectrum of Ru(bpy)32+ in aqueous and acetonitrile solutions. J. Photochem. Photobiol. Chem. *70*, 29–33. https://doi.org/10.1016/1010-6030(93)80005-T.

63. Goez, M., von Ramin-Marro, D., Othman Musa, M.H., and Schiewek, M. (2004). Photoionization of [Ru(bpy)3]2+: a catalytic cycle with water as sacrificial donor. J. Phys. Chem. A *108*, 1090–1100. https://doi.org/10.1021/jp036790r.

64. Müller, P., and Brettel, K. (2012). [Ru(bpy)3]2+ as a reference in transient absorption spectroscopy: differential absorption coefficients for formation of the long-lived 3MLCT excited state. Photochem. Photobiol. Sci. *11*, 632–636. https://doi.org/10.1039/C2PP05333K.

65. DiMarco, B.N., O'Donnell, R.M., and Meyer, G.J. (2015). Cation-dependent charge recombination to organic mediators in dye-sensitized solar cells. J. Phys. Chem. C *119*, 21599–21604. https://doi.org/10.1021/acs.jpcc.5b07342.

66. Wehlin, S.A.M., Troian-Gautier, L., Li, G., and Meyer, G.J. (2017). Chloride oxidation by ruthenium excited-states in solution. J. Am. Chem. Soc. *139*, 12903–12906. https://doi.org/10.1021/jacs.7b06762.

67. Kurtz, D.A., and Dempsey, J.L. (2019). Proton-coupled electron transfer kinetics for the photoinduced generation of a cobalt(III)-Hydride complex. Inorg. Chem. *58*, 16510–16517. https://doi.org/10.1021/acs.inorgchem.9b02445.

68. Frisch, M.J., Head-Gordon, M., and Pople, J.A. (1990). A direct MP2 gradient method. Chem. Phys. Lett. *166*, 275–280. https://doi.org/10.1016/0009-2614(90)80029-D.

69. Frisch, M.J., Head-Gordon, M., and Pople, J.A. (1990). Semi-direct algorithms for the MP2 energy and gradient. Chem. Phys. Lett. *166*, 281–289. https://doi.org/10.1016/0009-2614(90)80030-H.

70. Head-Gordon, M., and Head-Gordon, T. (1994). Analytic MP2 frequencies without fifth-order storage Theory and application to bifurcated hydrogen bonds in the water hexamer. Chem. Phys. Lett. *220*, 122–128. https://doi.org/10.1016/0009-2614(94)00116-2.

71. Head-Gordon, M., Pople, J.A., and Frisch, M.J. (1988). MP2 energy evaluation by direct methods. Chem. Phys. Lett. *153*, 503–506. https://doi.org/10.1016/0009-2614(88)85250-3.

72. Sæbø, S., and Almlöf, J. (1989). Avoiding the integral storage bottleneck in LCAO calculations of electron correlation. Chem. Phys. Lett. *154*, 83–89. https://doi.org/10.1016/0009-2614(89)87442-1.

73. Krishnan, R., Binkley, J.S., Seeger, R., and Pople, J.A. (1980). Self-consistent molecular orbital methods. XX. A basis set for correlated wave functions. J. Chem. Phys. *72*, 650–654. https://doi.org/10.1063/1.438955.

74. McLean, A.D., and Chandler, G.S. (1980). Contracted Gaussian basis sets for molecular calculations. I. Second row atoms, Z=11–18. J. Chem. Phys. *72*, 5639–5648. https://doi.org/10.1063/1.438980.

75. Frisch, M.J., Trucks, G.W., Schlegel, H.B., Scuseria, G.E., Robb, M.A., Cheeseman, J.R., Scalmani, G., Barone, V., Petersson, G.A., Nakatsuji, H., et al. (2016). Gaussian 16 Rev. C.01.

76. Tomasi, J., Mennucci, B., and Cancès, E. (1999). The IEF version of the PCM solvation method: an overview of a new method addressed to study molecular solutes at the QM ab initio level. J. Mol. Struct.: THEOCHEM *464*, 211–226. https://doi.org/10.1016/S0166-1280(98)00553-3.

77. Balawender, R., and Geerlings, P. (2001). Nuclear Fukui function from coupled perturbed Hartree–Fock equations. J. Chem. Phys. *114*, 682–691. https://doi.org/10.1063/1.1331359.

78. Cohen, M.H., Ganduglia-Pirovano, M.V., and Kudrnovský, J. (1994). Electronic and nuclear chemical reactivity. J. Chem. Phys. *101*, 8988–8997. https://doi.org/10.1063/1.468026.

79. Cohen, M.H., Ganduglia-Pirovano, M.V., and Kudrnovský, J. (1995). Reactivity kernels, the normal modes of chemical reactivity, and the hardness and softness spectra. J. Chem. Phys. *103*, 3543–3551. https://doi.org/10.1063/1.470238.

80. Becke, A.D. (1988). Density-functional exchange-energy approximation with correct asymptotic behavior. Phys. Rev. A Gen. Phys. *38*, 3098–3100. https://doi.org/10.1103/PhysRevA.38.3098.

81. Lee, C., Yang, W., and Parr, R.G. (1988). Development of the Colle-Salvetti correlation-energy formula into a functional of the electron density. Phys. Rev. B Condens. Matter *37*, 785–789. https://doi.org/10.1103/PhysRevB.37.785.

82. Miehlich, B., Savin, A., Stoll, H., and Preuss, H. (1989). Results obtained with the correlation energy density functionals of becke and Lee, Yang and Parr. Chem. Phys. Lett. *157*, 200–206. https://doi.org/10.1016/0009-2614(89)87234-3.

83. Aprà, E., Bylaska, E.J., de Jong, W.A., Govind, N., Kowalski, K., Straatsma, T.P., Valiev, M., van Dam, H.J.J., Alexeev, Y., Anchell, J., et al. (2020). NWChem: past, present, and future. J. Chem. Phys. *152*, 184102. https://doi.org/10.1063/5.0004997.

84. Shan, B., and Schmehl, R. (2014). Photochemical generation of strong one-electron reductants via light-induced electron transfer with reversible donors followed by cross reaction with sacrificial donors. J. Phys. Chem. A *118*, 10400–10406. https://doi.org/10.1021/jp503901v.

85. Childs, H., Brugger, E., Whitlock, B., Meredith, J., Ahern, S., Pugmire, D., Biagas, K., Miller, M., Harrison, C., Weber, G., et al. (2012). VisIt: an end-user tool for visualizing and analyzing very large data. In High Performance Visualization-Enabling Extreme-Scale Scientific Insight, pp. 357–372.

86. Cauët, E., Bogatko, S., Liévin, J., De Proft, F., and Geerlings, P. (2013). Electron-attachment-induced DNA damage: instantaneous strand breaks. J. Phys. Chem. B *117*, 9669–9676. https://doi.org/10.1021/jp406320g.